Health Condition Monitoring of Civil Structures Using Time Varying Autoregressive Models

By
Justin Tombe Demetry

A thesis
Presented to Lakehead University
in Fulfillment of the
Thesis Requirement for the Degree of
Master of Science in Mechanical Engineering
(MSc-ME)

Thunder Bay, Ontario, Canada, 2017

© Justin Tombe Demetry 2017

ABSTRACT

In recent years, there have been an increasing interest in long-term monitoring of civil structures, as the research community has been alarmed by some tragic events and collapses of bridges and buildings that pointed out the vulnerability of some existing structures and the uncertainties in their analysis for monitoring and maintenance purposes. SHM is the measurement of the operating and loading environment; as well as the critical responses of a structure to track and evaluate the symptoms of incidents, anomalies, damage and/or deterioration which may affect operation, serviceability, safety and reliability. Although many damage detection techniques were applied to scaled models or specimen tests in controlled laboratory environments, the performance of these techniques in real operational environments is still questionable and needs to be validated. Often damage sensitive features employed in these damage detection techniques are also sensitive to changes of environmental and operation conditions of the structure. The objective of this study is to propose a new Time Varying Autoregressive (TVAR) modeling technique for SHM of large-scale structures like bridges and buildings. TVAR model, a method by virtue of its nature is applicable for modeling data whose spectral content varies with time. The research is conducted to critically understand the effective performance of the structures under various loads and health conditions, and detect their operational anomalies using the proposed data-driven technique. In this research, an attempt is made to alleviate the use of system identification method where TVAR modeling is conducted directly on the data. The proposed method does not depend on the complicated algorithms and free of any other user-defined parameters. In pursuance of applying the proposed data-driven technique, the data collected on site are essentially paramount. Data inherently used are mainly obtained from experiments, as well as the data acquired from the Harbin Institute of Technology in fulfillment of a full-scale validation. The proposed TVAR technique detects not only the occurrence of structural damage, but also the location of damage. Whereas the TVAR developed captures the changes in the time domain, for comparison, Stochastic Subspace System Identification (SSI) method is applied to the experimental data. The method is used because it is an important tool that captures the frequency changes, as the SSI tracks the changes in the frequency domain. Using both experimental and full-scale studies, it is shown that the proposed TVAR technique and the comparable SSI method applied, can therefore be considered as a useful tool for SHM.

ACKNOWLEDGEMENTS

First, I would like thank God the almighty for providing me with the opportunity and granting me the capability to proceed successfully with my studies despite all challenges painstakingly endured. This thesis completion is due to the assistance and guidance of many whom I am indebted to for their contribution, thus, like to offer my sincere thanks to all of them. Foremost, I would like to express my sincere gratitude to my supervisor, Dr. Wilson Wang, who had truly shown his hard and smart working habit, charisma, high professionalism, straightforwardness, thoughtful comments, encouragement, and the continuous support and guidance throughout my studies at LU. I will wholeheartedly treasure his immense empathy and generosity. Likewise, my gratitude goes to Dr. Ayan Sadhu, my great co-supervisor from the Department of Civil Engineering whom, despite the fact that I worked with him lately on this research, he had shown his patience, kindness and motivation using his immeasurable skills, knowledge and experience, which truly made me successfully complete the thesis. I could not have imagined having better and highly professional professors and mentors with great advice like Dr. Wang and Dr. Sadhu.

My appreciation also goes to the committee members, Dr. Jian Deng and Dr. Hao Bai for taking their time to evaluate my seminar, provide comments and review my thesis prior to preparation for my defense. I wish all the committee members the best in their field of academia and beyond.

My sincere gratitude to my loving, caring and warmhearted parents, mama Poni-na-Valantino and Ret. Eng. Demetry Jubek Lado. Without their love and support in placing me in the best schools throughout my studies at the primary, intermediate and senior level, I wouldn't have reached this stage of being dedicated and ever eager to achieve my full potentials. My appreciation also to my grandparents (RIP) and my great grandparents (RIP) who were truly special people in my life whom most of them have helped and advised me to be strong and resolute despite all the life challenges. I cannot forget my wonderfully loving brothers, sisters, relatives, in-laws and friends for their encouragement. Above all, my sincere gratitude goes to my loving wife Naila, and my adorable kids, Lado, Jata and Poni whom I have painfully left them so as to pursue my studies. Without my wife's love, support and her patient in keeping the fundamental of our family and the understanding in taking the challenge to care for our very young kids far away from where I study, I wouldn't have imagined how to embark or complete this program. I therefore owe them a lot in enduring my absence from home. Last but not least, I really appreciate and thank all my family members, relatives and friends for their patience and understanding while I alienated myself in pursuit of knowledge.

TABLE OF CONTENTS

LIST OF FIGURES

LIST OF TABLES

1. INTRODUCTION

The goal of the Structural Health Monitoring (SHM) technology is to understand the behavior of civil structures, evaluate the safety levels and make maintenance decisions making. The SHM is important in monitoring the safety of structures, and establishing the lifecycle performance strategies or techniques, so as to maintain the integrity of the structures to ensure public safety.

There are several proposed definitions of SHM; however, the most commonly accepted one for SHM is the measurement of the operating and loading environment; as well as the critical responses of a structure to track and evaluate the symptoms of incidents, anomalies, damage and/or deterioration which may affect operation, serviceability, safety and reliability [1]. Relatively, vast literature presents an extensive survey of various damage detection techniques in civil structures that utilize changes in modal properties such as natural frequency, damping and mode shapes [2].

Many damage detection techniques are developed in the last decades [3] which can be broadly classified based on the level of attempted identification: the presence, location, and the severity of the damage [4]. Recent development in signal processing tools has resulted in a paradigm shift in its application towards damage detection [3]; thereby, leading to a class of algorithms which employ different time-frequency transformation based approaches such as wavelets [5], empirical mode decomposition and Hilbert-Huang transform [6].

In time-domain approach for SHM, a number of linear time series models have been described in literature, but they only consider the linear Autoregressive (AR) models as an alternative benchmark to the nonlinear autoregressive models. By its very nature, the AR model specifies that, the output variable depends linearly on its own previous values [7]. Hence, in the time-domain methods, model properties are extracted either from time histories (direct methods), or from impulse response functions - which are the inverse Fourier transforms of the measured spectra (indirect methods) [8].

Another method which uses the same approach is the Eigen Realization Algorithm (ERA). It utilizes the structural vibration data to build a state-space system, in which the model parameters of the structure of interest can be identified from the experimental data. Fundamentally, as stated by Juang et al. in [9], ERA model is the state-space representation of a physical system of a set of input, output and state variables of a dynamical system. In case of the ERA method, a matrix containing the measured data is created first; then singular value decomposition is performed on the data matrix to determine the rank of the system and rebuild the reduced matrix; which in turn is used to calculate the state-space matrices. Finally the Eigen values and Eigen vectors or the modal properties are then calculated from the realized state-space matrices.

James et al. proposed the Natural Excitation Technique (NExT) in [10] for an input which is not measured, it can be assumed to be white noise – a broad-band random excitation with constant spectral density. The cross-correlation function between two response measurements is likewise an inverse Fourier transform of the Cross Power Spectrum (CPS), which can be expressed as the sum of the decaying sinusoids having the same frequencies and damping ratios as the modes of the system. Therefore time-domain methods such as the ERA can be applied to obtain the resonant frequencies. On the other hand, Stochastic Subspace Identification (SSI) is an output-only modal analysis time-domain method. As stated by Peeters et al. in [11], SSI can be considered as an enhanced ERA whereby the input is not measured but assumed to be a stochastic process with white noise.

The effects of damage in a structure are classified as linear or nonlinear [2]. In essence, a linear damage situation is defined as the case when an initially linear-elastic structure remains linear-elastic after damage. Therefore, changes in modal properties primarily occur due to the changes in geometry and/or the material properties of the structure. Consequently, the structural response can still be modeled using a linear equation of motion [2].

Time-series models can be used to characterize the sources that are obtained from the past observations, followed by the future sources which are the predicted measurements [12]. With the arrival of newer measurements which contain the signature of structural damage, if some clear difference can be observed between the predicted and true measurements, it indicates damage. Once the damage is detected, the modal parameters of the damaged state are updated based on the new measurements. As a result, the damage and the undamaged modal parameters are estimated in an adaptive fashion [13].

In general, the long-span bridges accommodate a number of vehicles concurrently, and therefore, are subjected to strong bridge-vehicle dynamic interactions. On the other hand, traffic loads on the long-span bridges such as the cable-stayed and suspension bridges are subjected to wind excitations, which make them experience complicated dynamic loads from both the bridge stochastic traffic and wind [14]. Such stochastic nature of wind and traffic, as well as the dynamic interactions, creates fatigue damage on bridges during their lifetime. Since the wind and the daily traffic load on bridges have a significant impact on their strength and serviceability [14], their fatigue damage can be categorized as a result of the following:

(1) Bridge and vehicle interactions;

(2) Bridge and wind interactions;

(3) Vehicle and wind interactions;

(4) Wind and vehicle interactions.

As a result of the above impacts to the structures, in recent years, there have been an increasing interest in long-term monitoring of bridges, as the research community has been alarmed by some tragic events and collapses of bridges that pointed out the vulnerability of some existing structures and the uncertainties in their analysis for monitoring and maintenance purposes. Some researchers have proposed the design approaches of SHM systems for cable-stayed bridges. Essentially, a SHM systems includes the following modules: data acquisition, signal transmission, data

management, data analysis, safety evaluations and alarm. A SHM system also contains functions such as a user interface, software developing configurations, and the software operational environment configurations [15].

In vibration-based SHM, damage identification is performed from time histories that are measured simultaneously with several vibration sensors (e.g., accelerometers) or strain gauges at different structural locations. Structural damage detection can then be performed in the time-domain from signal analysis; damage-sensitive features are first extracted from the time series for SHM. The impediment of frequency-domain is the difficulty to distinguish between peaks that represent natural frequencies, those due to excitation, and the difficulty to identify closely spaced modes. Time–frequency also show too much redundancy and do not exhibit significant features related to damage [16].

Research on the design approaches of SHM systems from many research papers which include data analysis, modeling, SHM technology safety evaluation; as well as the summary of applications of the SHM technology for the cable-stayed bridges and the building structures have generated a great desire to use the Time Varying Autoregressive (TVAR) modeling techniques because it is essential for the development of the long-term continuous vibration-based SHM of structures.

1.1. Organization of the Thesis

The remaining ineludible work is organized as follows: Chapter 2 comprises of literature review, which focuses on SHM related research in general, and the time-domain approach for SHM in particular. Problems are then recognized and the objectives, strategies and significance are introduced. For Chapter 3, the emphasis is on the proposed methodology, the methodology flowchart, and the contribution. Chapter 4 encompasses the experimental validation of the 6 DOF model A and the 5 DOF model B. The description, testing set-up, results and conclusion for both

models are covered in this chapter. Chapter 5 is mainly on the full scale validation, which includes description, established monitoring system, and the results of the data acquired from Harbin Institute of Technology (HIT). This vibration data was extracted from a full scale bridge in China. Chapter 6 covers the Stochastic Subspace System Identification technique used for comparison; whereas Chapter 7 comprises of the summary, key conclusions and future work.

2. LITERATURE REVIEW

2.1. General Overview of Structural Health Monitoring (SHM)

Bridge health monitoring programs have historically been implemented with the aim of understanding and eventually calibrating models of the load–structural response chain. Carder et al. in [17] documented the earliest systematic bridge monitoring system on Golden Gate bridge, and the San Francisco-Oakland Bay bridge, in an elaborate program of measuring periods of various components during their construction. The purpose was to learn about the dynamic behavior and possible consequences of an earthquake.

A University of Washington report in [18] describes the monitoring of the first Tacoma Narrows bridge over its short life before it collapsed due to wind-induced instability. The focus was on the vibration measurements, but with an obviously warranted concern for the health of the structure. The Tacoma Narrows experience has far reaching importance since almost all of the long-span suspension bridge monitoring exercises to date have been related to concerns about wind induced response and possible instability.

The Tacoma incident occurred on November 7, 1940 near Seattle, USA, whereby, with the wind velocity of about 60 Km/h, the bridge twisted about 45 degrees in two waves, and oscillated violently up and down one meter in nine waves. According to Levy et al. in [19], the oscillations reached 8 meters as the bridge tore itself apart as per Figures 2.1 and 2.2. The Federal Works Agency investigated the collapse found that the bridge was well designed and well built. While it could safely resist all static forces, the wind caused extreme undulations which led to the bridge's failure. The failure was due to the bridge's design reacting to the wind, and the collapse is described as a simple case of resonance.

Figure 2.1: The start of the collapse of Tacoma Narrows bridge [19].

Figure 2.2: After the collapse of Tacoma Narrows bridge [19].

The collapse of the Tacoma Narrows bridge is perhaps the best recorded and documented bridge failure in the history of bridge engineering. The prolonged failure process was captured on extensive live footage, giving a unique document for the investigation committee, as well as the engineering society at large. Even though the Tacoma Narrow incident is not directly related to

SHM, the footage however since then has been used in civil engineering classes all around the world for educational purposes, as it is a very instructive video showing the consequences of neglecting dynamic forces in the design and construction of civil structures such as bridges [19].

Another unfortunate incident likewise took place in 2007 where there was a bridge collapse on the Interstate 35W Mississippi River, officially known as Bridge 9340 in Figures 2.3 and 2.4, an eight lane steel truss arch bridge which carried I-35W across the Saint Anthony falls in Minneapolis, Minnesota, USA [21]. During the evening rush hour on August 1, 2007, it suddenly collapsed and consequently killed 13 people and 145 were injured. According to the National Transportation Safety Board in [22], inadequate capacity for the expected loads on the structure initiated the gusset plates on the center portion of the deck truss to fail, which resulted in the collapse. The tragic incident have raised many concerns regarding the current condition of bridges, and also served as reminder of the necessity to develop rational and practical methods for SHM.

Figure 2.3: During the collapse of 35W bridge [21].

Figure 2.4: After the collapse of 35W bridge [21].

2.2. Excerpt from the shocking 9/11 World Trade Center Attack

Another devastatingly unforgettable event that shocked the world was the World Trade Center (WTC) attack on September 11th, 2001, when two commercial aeroplanes were hijacked by terrorist, then crashed into the two WTC towers in Figure 2.5. Each WTC building was 110 stories, and were built to withstand extreme conditions such as hurricane force winds, sabotage of external columns, and even collision from a medium size aircraft. With the 9/11 incident, however, the explosion damage coupled with the extreme heat from the fires weakened the steel beams and the columns until they buckled. When the collapse initiated, the dynamic impact of each floor led to progressive failure of all the columns, which resulted in the complete destruction of both towers, and consequently contributed to a catastrophic 2,800 loss of lives [23].

Figure 2.5: Collapse of WTC tower 2 after the 9/11 terrorist attack [21].

Research by Usmani et al. in [23] have shown that the structural system adopted for the twin-towers may have been unusually vulnerable to a major fire. A robust but simple computational and theoretical analysis has been carried out to answer some questions. As per Usmani et al. in [23], all results presented can be checked by any structural engineer either theoretically or through widely available structural analysis software tools. The paper stated that the analysis results showed a simple but unmistakable collapse mechanism that pointed out more to the geometric thermal expansion effects, as it does to the material effects of loss of strength and stiffness. The collapse mechanism discovered is a simple stability failure directly related to the effect of heating as a result of fire. Such studies resonates with the need for the SHM to ensure structural integrity in order to save lives.

2.3. Review of SHM

A comprehensive reviews of the technical literature concerning the detection, location, and characterization of structural damage via techniques that examine changes in the measured

structural vibration response was conducted by Doebling et al. in [24]. For example in [2], neural networks (NN) are used to estimate and predict the extent and location of damage in complex structures. A commonly applied NN is the multilayer perceptron trained by backpropagation, a system of cascaded sigmoid functions whereby, the outputs of one layer multiplied by weights, summed and shifted by a bias are used as the inputs to the next layer.

After the architecture for the network is chosen, the actual function represented by the NN is encoded by the weights and biases. The backpropagation learning algorithm is to adjust the weights and biases by minimizing the error between the predicted and measured outputs. There are typically more adjustable weights than experiments, and the body of data is repeatedly run through the training algorithm until some criterion for training is satisfied [2].

Almost all of the reviewed soft-computing-based approaches suffer from a common drawback, which requires a large data sets from both the undamaged and damaged structures for training, which may be hardly available from real world structures [25]. Likewise, the accuracy of the NN models depends on how it is trained to solve new problems. Other issue associated with the biological approach is that, a poorly trained model using sparse or corrupt data could lead to inaccurate results [26]. Review by Doebling et al. in [2] shows that, the main obstacles for deploying a monitoring system in field is the environmental and operations variation of the structure. Although many damage detection techniques were applied to scaled models or specimen tests in controlled laboratory environments, the performance of these techniques in real operational environments is still questionable and needs to be validated. Often damage sensitive features employed in these damage detection techniques are also sensitive to changes of environmental and operation conditions of the structure [25].

2.4. Related SHM Technique for Damage Detection

In general, damage detection employed in different fields of engineering are the conventional model-based approaches, soft-computing approaches such as the NN and genetic algorithm (GA), Signal processing-based approaches which includes wavelets, Chaos theory and the Multi-paradigm approaches [26]. Paper [2] presents an extensive survey of many damage detection techniques in civil structures. Damage indicators are primarily based on changes in the model parameters that reflect equivalent variations in the physical parameters of the system. The alterations in physical parameters commonly occur due to structural degradation under various environmental conditions, human-induced excitation or natural events, such as earthquake and strong winds.

Many damage detection techniques are developed in the last decades [3] which can be broadly classified based on the level of attempted identification: the presence, location, and the severity of the damage [4]. Recent development in signal processing tools has resulted in a paradigm shift in its application towards damage detection [3]; thereby, leading to a class of algorithms which employ different time-frequency transformation based approaches such as wavelets [5], empirical mode decomposition and Hilbert-Huang transform [6].

Finite-element method is a conventional model-based approach typically done through computer modeling of the structure. It identifies structural parameters using data acquired from the field or laboratory. Its main advantage is the conducive modeling and estimation of the physical properties; whereas its convenience factors are the ability to use commercially available software such as MATLAB to create and maintain the structural model.

Wavelets and other signal processing approaches have been utilized for their ability to retain time and frequency information to solve complicated time series pattern recognition problems in civil engineering [27]. A few researchers have employed the Chaos Theory and its fractal concept to model complicated structural dynamics, and estimate the fatigue damage in Fiber

Reinforced Polymer (FRP) stay cables using acoustic emission technique, and the fractal concept from the chaos theory [28]. Multi-paradigm approach integrates two or more computing paradigms such as NNs, fuzzy logic, evolutionary computing or GA, and the signal processing techniques such as the wavelet transforms, for nonlinear and complex problems [29].

The effects of damage in a structure are classified as linear or nonlinear [2]. In essence, a linear damage situation is defined as the case when an initially linear-elastic structure remains linear-elastic after damage. Therefore, changes in model properties primarily occur due to the changes in geometry and/or the material properties of the structure. Consequently, the structural response can still be modeled using a linear equation of motion [2].

Time-series models can be used to characterize the sources that are obtained from the past observations, followed by the future sources which are the predicted measurements [12]. With the arrival of newer measurements which contain the signature of structural damage, if some clear difference can be observed between the predicted and true measurements, it indicates damage. Once the damage is detected, the model parameters of the damaged state are updated based on the new measurements. As a result, the damage and the undamaged modal parameters are estimated in an adaptive fashion [13]. Rytter in [4] classified the various methods based on the level of identification attempted, which are:

- Level 1: determines the damage in the structure;
- Level 2: determines the geometric location of the damage;
- Level 3: quantify the severity of the damage;
- Level 4: predicts the remaining service life of the structure.

Although real damage in a structure can either be localized or distributed, model-updating techniques are generally more suitable for distributed damage events. The use of a large number of individual damage parameters coupled with a limited amount of measured data can lead to difficulties in convergence and non-uniqueness of solutions in updating algorithms [4].

2.5. Statistical Damage Related Technique - Kurtosis

Root Mean Square (RMS) is commonly used time-domain feature which measures the energy content of a signal. Likewise, statistical moments such as the mean, variance, skewness, and kurtosis are often used to process raw time-series data. Kurtosis is the normalized fourth moment that describes the relative spikiness and flatness of a distribution as compared to normal distribution, and it can be utilized as an important feature in representing fault condition. Kurtosis of a random variable is defined as the normalized fourth central moment, i.e.

$$K = \frac{E(x - \mu)^4}{\sigma^4} \tag{2.1}$$

where E is the expectation operator, μ and σ is the mean and standard deviation respectively. A distribution with kurtosis higher than 3 is referred to as Leptokurtic, and when the kurtosis less than 3 is Platykurtic; whereas for the Gaussian distribution, the kurtosis is 3 and is called Mesokurtic [30]. Kurtosis greater than 3 indicates more data far from the mean or some peaks can be observed in data distribution. If the kurtosis is less than 3, the data distribution is flat with short tails.

2.6. Time Domain Approach for SHM

In the time-domain methods, model properties are extracted either from time histories (direct methods), or from impulse functions - which are the inverse Fourier transform (FT) of the measured spectra (indirect methods) [8]. Another method which uses the same approach is the Eigen Realization Algorithm (ERA). It utilizes the structural vibration data to build a state-space system, in which the model parameters of the structure of interest can be identified from the experimental data.

Fundamentally, as stated by Juang et al. in [9], ERA model is the state-space representation of a physical system of a set of inputs, output and state variables of a dynamical system. In the case of ERA, a matrix containing the measured data is created first, and then singular value

decomposition is performed on the data matrix to determine the rank of the system and rebuild the state-space matrices. Finally the Eigen values and Eigen vectors or the model properties are calculated from the realized state-space matrices.

The dynamic model of a structure can be described by a set of linear differential equations:

$$M\ddot{\mathrm{U}}(\mathrm{t}) + C\dot{\mathrm{U}}(t) + K\mathrm{U}(t) = F(t) \tag{2.2}$$

where *M*, *C* and *K* are the mass, damping and stiffness matrices; whereas U*(t)* and *F(t)* are the displacement and input force vectors; *(*$\dot{\mathrm{U}}$*,* $\ddot{\mathrm{U}}$) are displacement derivatives with respect to time [31]. Alternatively, Eq. [2.1] can be re-written in a state-space representation as a set of first-order differential equations:

$$\dot{\mathrm{x}}(t) = A_c x(t) + B_c u(t) \tag{2.3a}$$

$$y(t) = C_c x(t) + D_c u(t) \tag{2.3b}$$

where the state vector *x(t)* and force vectors *F(t)* are:

$$x(t) = \begin{Bmatrix} \mathrm{U}(t) \\ \mathring{\mathrm{U}}(t) \end{Bmatrix} \tag{2.4a}$$

$$F(t) = B_2 \mathrm{u}(t) \tag{2.4b}$$

The vectors u(*t*) and *y*(*t*) represent observations of the input and output of the process respectively, A_c is the state matrix which represents the dynamic characteristics of the system, and the B_c is the input matrix which represents the input influence; C_c is the output matrix which specifies how system states are transformed to the output, while D_c is the output control or the direct feed-through matrix, and the subscript *c* denotes continuous time. Hence, a discrete time state-space model becomes:

$$x_{k+1} = Ax_k + Bu_k \tag{2.5a}$$

$$y_k = Cx_k + Du_k \tag{2.5b}$$

where *k* is an index which identifies a specific time increment.

In practice, there is always noise with random variables (measurements), which can be divided into process and measurement noise. The process noise is due to disturbances in the input, whereas the measurement noise is due to the inaccuracy in sensor readings. The state-space model can therefore be extended to include these stochastic components, as follows:

$$x_{k+1} = Ax_k + Bu_k + w_k \tag{2.6a}$$

$$y_k = Cx_k + Du_k + v_k \tag{2.6b}$$

where w_k and v_k are the disturbance and measurement noise respectively, both of which are assumed to resemble white noise.

A graphical representation of the system in state-space terms is shown in Figure 2.6. It shows the vector signals u_k and y_k are measurable or in other words, observed. While v_k and w_k are the unknown disturbances with noise, the symbol Δ represents a delay.

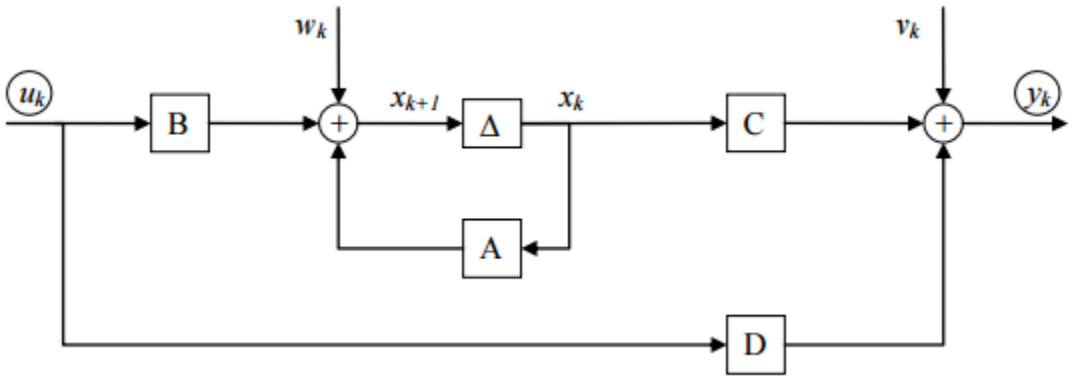

Figure 2.6: State-space system [31].

In the civil engineering structural testing, only the response y_k of the structure is usually measured, and therefore, it becomes impossible to distinguish the input term u_k from the noise term w_k in Eq. [2.6a], which result in the output-only stochastic system [31]:

$$x_{k+1} = Ax_k + w_k \tag{2.7a}$$

$$y_k = Cx_k + v_k \tag{2.7b}$$

2.7. Frequency Domain Methods

Frequency-domain methods make use of the FT spectra of measured signals to extract the modal properties [32]. As per the basic principles of structural dynamics, a structure will vibrate either at one or more of its own natural frequencies, or at the frequencies induced as a result of forced vibrations. When a structure is excited by a force with a flat spectrum in the frequency range of interest, the structure will vibrate most vigorously at its own natural frequencies due to resonance.

The resonant vibration will be manifested as peaks in the structural response spectra corresponding to the structural natural frequencies. It therefore becomes possible to look at the response spectra from an FT analysis, then check for peaks that correspond to the damped natural frequencies of the structure, a technique referred to as 'The Peak Picking' [32]. Once the natural frequencies are identified, the relative model amplitudes at various measurement locations can then be computed to estimate the vibration mode shapes [33]. The impediment of this method includes the difficulty to distinguish between peaks that represent natural frequencies, and those due to excitation, as well as the difficulty to identify closely spaced modes [34].

In ambient vibration measurements such as the bridge vibration testing, it is impossible to measure the time history of the input force due to ambient excitation such as that caused by traffic or wind loading. It is the reason why only the spectra of bridge responses are measured and then used to extract the structural model properties. The response of the structure at one location is then used as a reference to scale the responses at other locations so as to calculate the mode shape amplitudes. For more accurate estimate of model properties, the Cross Power Spectrum (CPS) approach is often used, which is considered as a product of the spectra of a reference accelerometer, and that of another accelerometer [35].

CPS represents the measure of the power that two signals have in common at specific frequencies [35]; the two measured responses will be correlated only at frequencies common to

both signals. The peaks retained in the CPS are those common to both signals, and are more likely to be true natural frequencies. The natural frequencies can then be estimated using visual inspection to locate the peaks in the CPS. Mode shapes are subsequently estimated from the relative magnitudes of these peaks at different locations on the structure. Another enhancement to the peak picking method is to apply Singular Value Decomposition to the cross spectral matrix, which can reduce the influence of noise in the signal [11]. These signal processing techniques [32] are described below:

For a time series $x(t)$, its FT (Spectrum), $X(f)$., is defined as:

$$X(f). = \int X(t)e^{i2\pi ft}dt \tag{2.8}$$

where t and f are time and frequency variables, respectively.

The Auto Power Spectrum of $X(f)$., $APS(X)$, is then written as:

$$APS(X) = X(f).X(f).^{*} \tag{2.9}$$

where * denotes the complex conjugate.

The CPS of the time series $x(t)$ and another time series $y(t)$ is defined as:

$$CPS(X,Y) = Y(f)X(f).^{*} \tag{2.10}$$

where $Y(f)$ is the spectral function of $y(t)$. Hence, the frequency response function, $H(f)$, may then be defined as:

$$H(f) = \frac{X(f).}{F(f)} \tag{2.11}$$

where $F(f)$ is considered to be the spectrum of the input force, and $X(f)$., represents the spectrum of the structure response [36].

2.8. Overview of the SHM Systems of Stayed Bridges

Some researchers have proposed the design approaches of the SHM systems for cable-stayed bridges, which include the objectives, modules and the functions of structural health

monitoring systems. Essentially, a SHM systems includes the following modules: data acquisition, signal transmission, data management, data analysis, safety evaluations and alarm. A SHM system also contains functions such as a user interface, software developing configurations, and the software operational environment configurations [15].

2.8.1. Design of Sensor Modules and Sensing Technologies

The design of sensory module of SHM systems for cable-stayed bridges comprises of the variable type, the sensor type, and the positioning of the installed sensors. The monitored variables can be categorized into three types: loads and environmental actions, global responses, and local responses. As per Li and Ou in [15], the loads and the environmental actions mainly include vehicle loads, wind velocity, earthquake ground motion, vessel collisions, temperature, humidity, rainfall intensity, chloride ion concentration, and CO_2 concentration.

The acceleration, deformation, and tilt are global response variables; whereas the strain, cable tension force, displacement and wears of joints and bearings, fatigue and crack of elements, corrosion of elements, and scour around piers are the local response variables. The vehicle loads including the weight of each axle, number of axles, and vehicle speed are frequently measured by weigh-in-motion (WIM) systems embedded in all lanes at a cross section of a cable-stayed bridge; the WIM systems can provide the vehicle load information at one cross section only [15].

Bao et al. in [37] proposed an approach to identify the spatial–temporal distribution of vehicle loads on a cable-stayed bridge through a compressive sensing technique based on monitoring of the cable tension force. In order to improve the identification accuracy, Chen & Cai in [14] proposed an identification method of the spatial-temporal distribution of vehicle loads on a cable-stayed bridge by combining WIM systems with cameras that is validated through the identification of location and time of heavy trucks on the Hangzhou Bay Bridge, which is a cable-stayed bridge in China.

The earthquake ground motion in three directions can be monitored by seismometers; however, the seismometers should be installed at the free-field away from the bridge, and on the piles of bridge piers. For long-span cable-stayed bridges, seismometers should be installed at more than one pier so as to investigate the travel wave effects. The vessel collisions can be measured by accelerometers, or by the seismometers on the piles of bridge piers [14].

Wind is one of the critical loads for long-span cable-stayed bridges; it excites vortex induced vibration of the decks and cables. Anemoscopes or ultrasonic anemoscope can be used for fluctuating winds, whereas propeller anemoscope can be employed to measure wind velocity. Due to rain-wind-induced stay cables vibration, rainfall intensity is a critical variable which can be measured by a rainfall gauge installed on the bridge without any shield [38].

For temperature measurements, thermocouples or optical fiber Bragg grating (FBG) sensors are frequently employed to measure the temperature around and inside the bridges. To ensure the survival of FBG sensors during construction of the civil structures, Ou and Li in [39] proposed embedded FBG sensors into fiber reinforced-polymer bars, which results in FRP bars with self-sensing properties and better mechanical performances. The location of temperature sensors is determined based on a thermodynamic analysis of the bridge.

The temperature sensor arrays should be embedded into the concrete elements so as to obtain the temperature gradient along at least one cross-sectional height. Due to the temperature compensation requirement of a strain gauge, temperature sensors should be installed close to strain sensors. On the other hand, the humidity is frequently monitored by hygrometers installed inside a box on the bridge girders. The chloride ion concentration can be measured by electrode probes, whose arrays are embedded in the cover of reinforced concrete piers [15].

Displacement or acceleration should be monitored for cable-stayed bridges by accelerometers with low-frequency bands. The location of accelerometers on the bridge deck can be determined by some placement optimization approaches. Accelerometers should be attached to

the long cables rather than the short cables because long cables are more prone to dramatic vibrations [15]. Transportation Research Board of the National Academies of the USA in [40] has indicated that security cameras mounted on the tower are proposed to monitor vibration of stay cables; however, there have been no indication of this technique practically used in monitoring of rain-wind induced vibration of stay cables.

For the tower, accelerometers should be attached to the top of the towers in two horizontal directions. The deformation of the tower can be measured by a global positioning system (GPS) and a tilt meter, whereas the deformation of a girder is usually monitored by GPS and hydraulic pressure connecting the pipe system [15]. Since strain is one of the most important variables for direct safety evaluation, fatigue assessment, and validation of the design, strain can be monitored using traditional strain gauges, vibrating-wire strain gauge, and the FBG strain sensors. Vibrating-wire strain gauges can only measure the static strain, which is why, in China, FBG strain sensors have been installed on many cable-stayed bridges for strain monitoring, such as the one installed on the Shandong Binzhou Bridge, a 3-tower cable-stayed bridge, as well as Jiashao Bridge that is a 6-tower cable-stayed bridge [41].

Dascotte in [42] proposed a method to derive strain from the displacement measured by a GPS system for accumulated fatigue assessment; however, the location of the strain sensors needs to be determined based on a structural analysis and fragility analysis. It further stated that, stay cables are the most critical elements in cable-stayed bridges because of their effect on steel wires and anchorage. The monitoring variables of the stay cables include vibration, tension force, fatigue damage, and corrosion.

Load cells can be installed at the anchorage of the cable, or a single strand; however, these cells are hard to replace. Zhang et al. in [43] proposed a method that employs smart sensors based on the elasto-magnetic (EM) and magneto-electric effect to monitor the stress of steel cables. The design theory of the sensor involves the EM coupling effect and magneto-electric coupling effect.

The potential of the elasto-magnetoelectric sensor as a non-destructive evaluation tool for monitoring cable stress was verified in a full-scale experiment with high sensitivity in [43]. Since EM sensor is sensitive to the cable cross section and size, it is implemented into the stay cables of the Adige Bridge in Italy [44].

The sensor life-span is estimated for 50 years, whereas the operational temperature range is between -20 to +80 °C, and the sampling rate can be 10 seconds [44]. Although the EM sensor can be easily replaced, it can only measure the static cable tension force, and cannot monitor the cable tension force in real time because of the demagnetization effect; that is why the Fiber optical sensors have been proposed to monitor cable tension force [44].

Another solution for monitoring cable frequencies from large distance is using laser vibrometer [45], which can speed up the vibration process. Suffice to say, the feasibility of this technique has been validated in [45]. The assumption on the chord may not reflect the actual cable boundary conditions and nonlinearity of cables caused; therefore, Kurz et al in [46] analyzed the existing non-destructive testing methods, and commented on a suitable approach for different scenarios of cable elements. Methods for the accessible parts include magnetic inspection and acoustic emission monitoring. Suitable techniques for monitoring the non-accessible parts include ultrasonic guided waves - particularly for anchorage zones, magnetic flux leakage inspection, micro magnetic method, and the acoustic emission method.

Corrosion of reinforced bar in concrete can be monitored based on the electrochemical response mechanism. Qiao et al. in [47] developed corrosion sensors, recognition algorithms, corrosion control actuators, for the internet-based durability monitoring. These components realize the assessment of safety, maintenance and reinforcement, as well as the performance-based design of the major infrastructures. Alternatively, Zhao et al. in [48] proposed to wrap the optical fiber sensors on reinforced bars to measure the expansion of concrete caused by corrosion, so as to diagnose corrosion locations and corrosion extent of reinforced bars.

2.8.2. DAQ, Transmission, Management, and User Interface

The design of data acquisition module includes selecting the transmission technology, data acquisition (DAQ) devices, and the sampling modes. In [49], analog signals can be transmitted to DAQ devices directly through shielded cables before analog-digital (A/D) conversion. Since the transmission distance should be limited because of the signal attenuation, direct analog signal transmissions are often used over short distances.

For the long transmission distance range, analog signals can be first converted to a digital signal, and then transmitted through industrial communication buses such as ethernet, PROFIBUS, RS-485, and wireless transmission techniques [15]. The communication bus can also be used by other automatic devices. Wireless transmission techniques have been applied in SHM including WiFi and ZigBee, whereas for the long distances, microwave communication is more appropriate [15].

DAQ devices contain signal conditioning devices; however, non-standard signals must first be conditioned through amplification, filtering, isolation, and any other processes. DAQ devices are determined according to the type and number of sensors and signals, and proper sampling rates, whereby, they can be connected with analog signals and digital signals when they are extended to the other interfaces [15]. For example, signals from FBG sensors may be collected by DAQ, whereas the static signals such as the strain and temperature can be collected by serial devices like the RS-232-based devices. The selection of sampling modes and the sampling rate are important when executing DAQ tasks [15].

An appropriate sampling rate is required to avoid huge and redundant data in the following fashion: data are sampled at specific time period each day, sampled when exceeding the threshold only, and sampled when a special event occurs. For instance, data are sampled after a typhoon, earthquake, vessel collision, or attack to the bridge; therefore, all data are sampled at a sampling rate. On the other hand, only typical data are saved and the remaining data are deleted [15].

For the dynamic and wave propagation signals, the sampling rate should follow the Nyquist– Shannon sampling theorem. Additionally, for the case of the static signal, the sampling rate can be determined according to the variation characteristics of the signals [15].

2.8.3. SHM System's Reliability

Given the fact that the lifetime of sensors is typically much shorter than that of the infrastructure, sensors must be long-term qualified, and might need to be replaced with new sensors during the life cycle of a structure. The reliability of both the sensing system and the monitoring data must be evaluated, and their uncertainties be also measured [50].

2.8.4. Real Time Monitoring of the 2nd Jindo Bridge

Figure 2.7 shows the instrumentation diagram for the online real time monitoring, which represents the general flowchart of the possible approach [51]. Essentially, static and dynamic types of sensors could be used for each monitoring project, whose data lines can be connected to the main data acquisition center at the bridge site. It was suggested in [51] that the data center can function 24 hours a day, 365 days a year, and should be capable of acquiring all the data concurrently, then synchronize and transfer the data to any remote location over an internet gateway.

The data center needs to have the capability of recording the data locally based on the preset trigger conditions, and also need to be monitored continuously at one or more remote locations. A real-time and continuous software based analysis can be carried out at the remote monitoring center, as a decision support system provider for the administrators and engineers in charge. For the warning messages, they need to be reported to the bridge administration immediately [51].

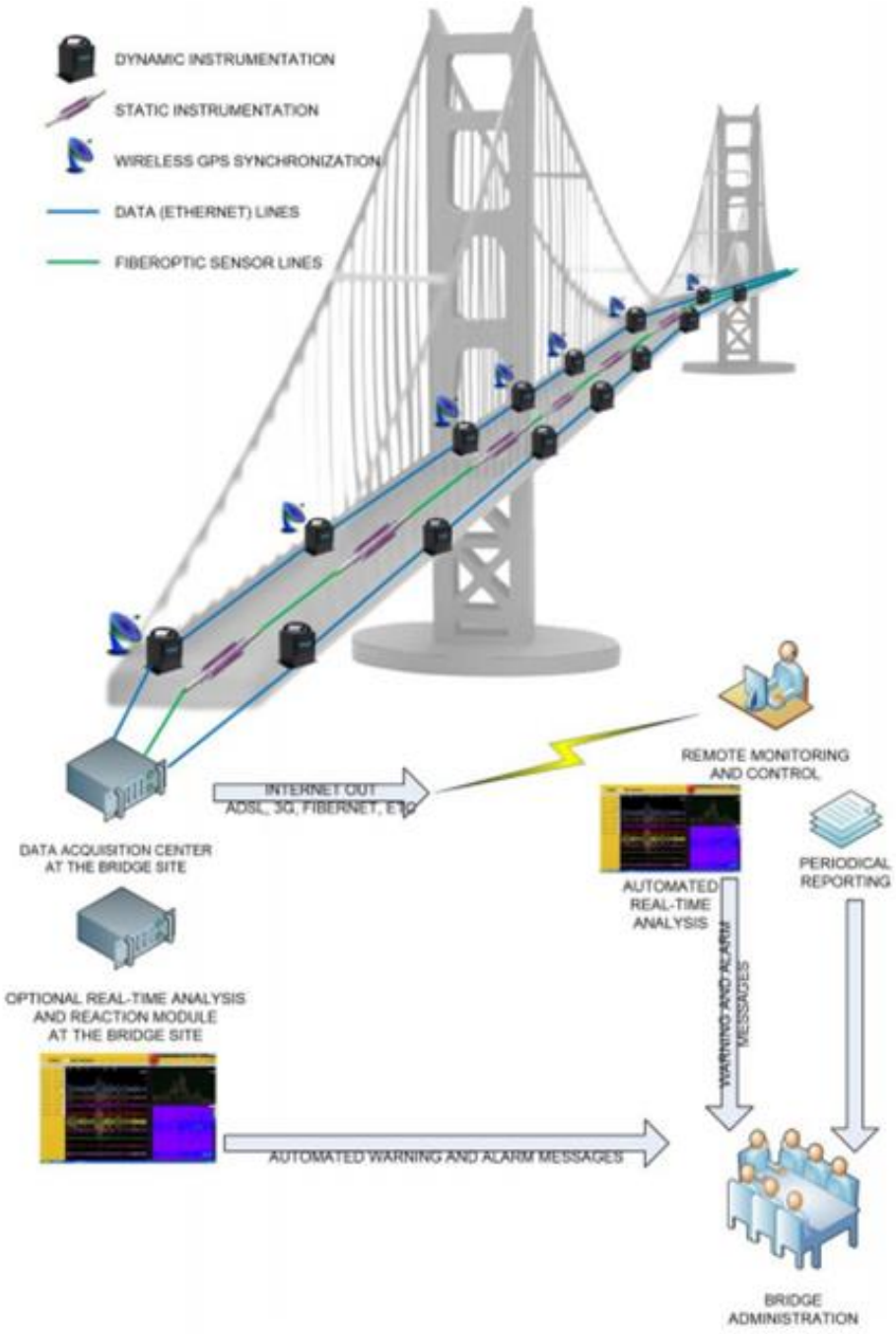

Figure 2.7: The general diagram of the suggested 7/24 real-time instrumentation approach [51].

Problems that are recognized with the existing SHM techniques in [24, 25] include the dependence of many methods on prior analytical models for the detection and location of damage. Almost all of the damage-identification methods reviewed were on some type of a linear structural model. The number and location of sensors were another important issue that was not addressed to any significant extent in the previously reviewed literature.

The literature was also found to have scarce instances of studies whereby, different health-monitoring procedures were compared directly through application to common data sets. Additionally, many research appeared not to be focused on testing of real structures in their operating environment, but rather on laboratory tests of simple structural systems in controlled environments [25]. On the other hand, the disadvantage of finite-element method is that, it does not produce accurate results for large and complex structures [26]. Many damage detection methods reviewed attempt to identify damage by solving an inverse problem, which inevitably requires the construction of analytical models [25]. Such a dependency, often uncertain and not fully validated with experimental data, makes these approaches less attractive for certain applications. Some researchers try to avoid this dependency on the numerical models by performing signal based unsupervised learning; however, these approaches could be effective for identifying the onset of damage, but they only identify the existence of damage [25].

2.9. Objectives, Strategies, Significance and Contribution

The objective of this study is to propose a new TVAR modeling technique for SHM of large-scale structures like bridges and buildings. The research is conducted to critically understand the effective performance of the structures under various loads and health conditions, and detect their operational anomalies using the proposed data-driven technique. In pursuance of applying the SHM technique, the data collected under various types of structures including experimental and real-life systems are essential, as it can help the validation of the proposed method. The TVAR-models are then used for analyzing data whose spectral content varies with time due to change in the properties or load of structures. The main advantages of damage detection in the time domain is that direct sensor data can be used without complex feature extraction.

In this study, the strategy is to use two different experimental models: 6-degree of freedom (DOF) building model, and a 5-DOF building model, both developed at the LU Civil Engineering

laboratory. The full scale validation is also performed with the aid of the benchmark study data provided by the Harbin Institute of Technology (HIT) in China. The research is conducted to systematically investigate the effective structural performance, detect performance anomalies, and localize damage to meet the standards for SHM. The significance of the proposed technique is to develop the practically effective and efficient approach of computing the time-varying parameters of degraded structures using the TVAR model, as well as the data from a full-scale structure, to prove that the model can work in both the laboratory environment and any real structure. Contributions of this work includes the following:

(1) Most of the SHM methods rely on system identification (ID) techniques where the vibration is decomposed into various modal components and then the respective model responses are investigated to evaluate the existing damages in the structure. However these methods are completely data-driven and the type of system ID method used becomes problem specific which requires enormous user discretion. In this research, an attempt is made to alleviate the use of system ID where TVAR modeling is conducted directly on the data. The proposed method does not depend on the complicated algorithms and free of any other user-defined parameters. The SSI method used is for comparison purposes only.

(2) Since TVAR modeling is employed directly on the raw data, model order selection becomes very critical. A new approach is proposed for model order selection. RMS values for each coefficient under undamaged and damaged case are determined as the time-domain features to measure the change in the energy content in a signal. The model order is selected by observing relative energy distribution of the signal across various channels.

(3) The third contribution is related to damage localization, which is identified by considering the percentage difference in the energies of the signal of the damage and the undamaged data. The channel with the highest percentage difference is considered as the damaged location.

3. METHODOLOGY

3.1. TVAR Background

Time Varying Autoregressive (TVAR) models are used for modeling data whose spectral content varies along time [52]. TVAR models for non-stationary time series are the extension of autoregressive (AR) models for stationary time series. While AR models have time-invariant coefficients, TVAR models have time-varying coefficients to capture the non-stationarity. Therefore, the theoretical backgrounds for AR and TVAR models are the Wold decomposition theory and the Cramér decomposition theory, respectively [53].

Rao in [52] addressed the TVAR models in the pioneer paper in which three parameter identification methods were proposed: the spectral matching method, local least squares method, and the local maximum method. The evolutionary power spectral density (EPSD) was simply related to TVAR models without explanation; however, since 1970, TVAR models have been studied and applied in civil engineering. TVAR models constitute a class of non-stationary processes; therefore, justifying TVAR models for applications and improving parameter identification methods are the two main issues in the vast literature [53].

In the latest research on TVAR, Musafere [54] proposed blind source separation (BSS)-based TVAR modeling technique to detect discrete damage. The second-order BSS is employed first to obtain the mono-harmonic responses from the vibration data where each of the undamaged natural frequencies has a discrete change to its damaged counterpart. Since the modal responses are single-frequency components, the TVAR modeling with a low model order is utilized to track the damage instant and detect the severity of changes in the modal parameters. Thus, the complexities in selecting the appropriate model order of the time-series models are alleviated. However one of the limitations of this method is the prerequisite of BSS method which is indeed computationally intensive.

Theoretically, the TVAR coefficient could be of any form. TVAR coefficients need to slowly vary with time so that these TVAR models can have the spectral representations and their coefficient functions to be identified from one single sample [53].

According to Dahlhaus in [55], identifying TVAR coefficients is a statistical problem which normally involves three stages: identification, model selection, and verification. The principle of maximum likelihood is the theoretical setting for TVAR parameter identification. Prior to the identification procedure, a specific TVAR model has to be set, which includes choosing the TVAR order and parameterizing the coefficient functions by putting smoothness constraint on the coefficient functions. Thereafter, the optimal coefficients can then maximize the associated likelihood function [55, 56].

Identifying TVAR coefficients is analogous to fitting a curve model to a noisy data; therefore, a more complex model with more parameters is needed for the smaller error or larger likelihood. A simpler and smoother model with less parameters has higher probability to exist, and is therefore more desirable in practice. Hence, this fidelity versus smoothness trade-off can be chosen via numerous criteria such as the Akaike's information criterion (AIC) [57], whereby the best model has the minimum AIC. The uncertainty principle is also true in TVAR models in the sense that increasing the resolution in the frequency-domain is required so as to improve the TVAR order, whereas increasing the resolution in the time-domain needs more parameters to characterize the coefficients.

3.2. Time Series Models

In time-domain approach for SHM, a number of linear time series models have been described, but they only consider the linear AR models as an alternative benchmark to the nonlinear AR models. On the other hand, Vector Autoregressive (VAR) is essentially a time series model used to capture the linear dynamics among multiple time series [7]. The VAR models

generalize the univariate AR model by allowing for more than one evolving variable. The VAR requires prior knowledge about variables which can be hypothesized to affect each other inter-temporally. A VAR model describes the evolution of a set of k endogenous variables over the same time period as a linear function of only their past values. A VAR model with lag length p, denoted as VAR(p) is defined as:

$$y_t = c + A_1 y_{t-1} + A_2 y_{t-2} + \ldots + A_p y_{t-p} + e_t \tag{3.1}$$

where y_t is $k \times 1$ vector of endogenous variables and e_t is IID distributed white noise process term of the same dimension. The coefficient matrices A_1, ..., A_p are of dimension $k \times k$ and estimated through OLS. The lag length in VAR(p) model can be selected through using information criteria such as AIC or BIC [7].

3.3. Model Order Selection

Appropriate model order selection is crucial for TVAR modeling. As per the principle of parsimony, extra parameters shouldn't be used when not necessary when describing a dynamic process [58]. With noise presence, TVAR model can recognize several spectral peaks well; however, the changes in the model order makes it sensitive, thereby producing false spectral peaks in the event that an inaccurate model order is chosen. It is based on this reason that the selection of the model order is an important aspect in TVAR modeling.

On the accuracy of the TVAR model which is sensitive to the choice of model order, inappropriate model order only results in model parameters that will not characterize the underlying nature of the process, which can further result in an inaccurate representation of the signal. In essence, for model based spectral analysis, too low of a model order can result in smoothed spectral estimate, whereas too high of a model order gives rise to misleading spectral peaks [57, 59, 60].

In a nutshell, with a given order coupled with smoothness constant, the model of the TVAR can be established. The challenge is which model order works best, which is the main intimidating thing with TVAR modeling. Since a given order in tandem with the smoothness constant aids with maximizing the likelihood function, as well as minimizing the sum of squares of residuals, it is fair to say that the model that is best in terms of fitness can be reached at if the right model is chosen.

In the event that there are two models that fit the data well on equal basis, the simpler one with free parameters should be the best choice as it is determined to be more likely closer to the truth [60]. The purpose of model selection is to optimize the balance between the degree of exactness to the data and the model simplicity, which suits a model that is in close relationship to the true model [61]. Statistical techniques that have been used in the selection of TVAR model order are the Akaike's final prediction error (FPE) [57], the AIC [60], the Bayesian information criterion (BIC) [61].

3.4. The Autoregressive (AR) Model

Essentially, the AR model is composed of parameters which define the general structure of the model, and the coefficients which are realized by fitting the AR model to the data [62]. Despite the fact that visualization of the power spectral density (PSD) is a powerful inference tool, the primary advantage of the AR model is that, the underlying process that produced the observed data can be inferred directly from the AR parameters and coefficients without ever constructing a PSD plot or spectrogram [62].

In this work, the ultimate interest is in a group of solutions which is peculiar to the class referred to as TVARs [63]. In general, TVARs largely consist of a three-step process:

(1) Assuming a general structure for the AR model;

(2) Employing an adaptive filter framework for dynamic AR model estimation;

(3) Using the resulting TVAR model to infer the dynamics of the data [64, 65].

The choice of the adaptive filter framework can greatly affect the quality of the TVAR model estimates; the challenge related is to understand the assumptions of the adaptive filter, and how to ensure that the adaptive filter and data input are mutually compatible? Thereafter, derive and apply a fixed-interval Kalman smoother sequential estimator for the TVAR model. A Kalman filter based approach needs to be chosen over other adaptive filters for the wealth of existing theoretical and practical knowledge [63].

3.5. The AR process

In the observation interval $t \in (0, T)$, time is discretized such that the discrete time index, n, obeys the sampling interval equation $t = n\Delta$, $f_s = 1/\Delta$ which is the sampling frequency, and $J = T / \Delta$ which is the largest discrete time index. The $y(n)$ denote the measured signal, and $v(n)$ denote the zero-mean Gaussian measurement white noise with variance σ^2_v; whereas the operator x^* denote the complex conjugate value of x. Thus, the AR model of order p or AR(p) model can then be described as follows [64, 65]:

$$y(n) = \sum_{k=1}^{p} a_k y(n-k) + v(n), \tag{3.2a}$$

where the respective z-transform and the power spectral density (PSD) functions can be represented as,

$$y(z) = \frac{V(z)}{\left(1 - \sum_{k=1}^{p} a_k z^{-k}\right)} \tag{3.2b}$$

$$S(z) \equiv E\left[y(z)y^*(z)\right] = \frac{\alpha_v^2}{\left[\left(1 - \sum_{k=1}^{p} a_k z^{-k}\right)\left(1 - \sum_{k=1}^{p} \alpha_k^* z^{-k}\right)\right]} \tag{3.2c}$$

The relationship between the AR model order and the assumed structure of the data, as well as the AR coefficients ($a_1,\ldots,a_p$) specify the shape of the PSD. Hence, the denominator

of (3.2c) is referred to as the characteristic polynomial because it fully captures the behavior of the model. Once the polynomial is factored, the roots or the poles will indicate if $y(n)$ has unstable, oscillatory, or damped components [66].

The interest should be in the oscillatory components, which are given when two roots of the characteristic polynomial have non-zero imaginary components and are complex conjugates of each other. In practice, the model order p is generally constrained to be even in such a way that, when all the roots have complex conjugates amongst themselves, the PSD of an AR(p) process, $S(z)$, will be a multi-modal function that resembles a summation of peaks; whereby each peak represents a signal. The relative height, shape, and location of the peaks are therefore entirely determined by the poles of the transfer function; whereas the phase of the pole determines where the center of the peak is positioned on the frequency axis. The height and width of the peak are determined by the modulus of the pole. The shape of the PSD is only as valid as the data is stationary in structure, and that is why AR model need to be extended to a TVAR model so as to explicitly describe the temporally evolving harmonics of the time series [64, 65].

3.6. Instantaneous Frequency Estimation Using Fixed Interval Kalman

Some methods of estimation assume that a_k is fixed over time [67], but the analysis of non-stationary signals requires a time-varying approach such that, $a_k \rightarrow a_k(n)$. Therefore, the Kalman filter (KF) framework can be thought of as a sequential estimator that optimizes the AR model coefficients with incremental observations of the data, and Gaussian variability. KF version of the TVAR can be derived as follows: By writing the AR process in discrete state-space form, a representation that is convenient for formulating adaptive filters [63].

$$x(n) = x(n-1) + w(n), \tag{3.3a}$$

$$y(n) = C(n)x(n) + v(n), \tag{3.3b}$$

where $x(n) = [a_1(n),\ldots,a_p(n)]^T$ is the hidden or state variable which corresponds to the AR coefficients at discrete-time n; then $C(n) = [y(n-1),\ldots y(n-p)]$ is the observation transformation vector; whereas $w(n)$ is the state transition noise with covariance $\sum_w = I^{pxp}\sigma_w^2$, and $v(n)$ is the observation noise with covariance σ_v^2. Additionally, the diagonal form of $\sum_w$, is an assumption that allows the AR coefficients to evolve independently of one another, as well as simplifies the algorithm by reducing the number of parameters. Given the values for σ_w^2, σ_w^2, p, and the data $y(n)$, the KF estimates the variable $x(n)$ for each discrete-time point in the observation interval, $n \in [1, J]$. Hence, the one-step prediction equations use past information to predict the state variables, and their statistics under a zero mean Gaussian random variable fulfills the assumption [63]. Details of the respective equations 3.6 to 3.8 are shown in section 3.7.

3.7. Application of TVAR

This work can be primarily classified as a parametric damage detection method; whereby, it literally estimate the inherent parameters of the structure using frequency response functions [68], auto-regressive models [16], and the statistical information [69]. In addition, Nguyen in [65] described TVAR as a form of modeling which tracks the real-time changes of the model coefficients, thereby, revealing the faults in the structures. In an alternate approach, $y(n)$ represent the Mixed-Model Response (MMR) sources, and $v(n)$ denotes the zero-mean Gaussian measurement noise with variance σ_v^2 ; therefore, the AR model of order p can be represented as in equation 3.2a in section 3.5.

It is because of the non-stationary nature of the MMR sources that, a recursive modeling approach is required whereby, a_k becomes $a_k(t)$. Kalman filter is then utilized to estimate these time-varying coefficients, knowing the observations of the data [65]. The following equation is the discrete representation of the $a_k(t)$ coefficients, where $w(n)$ is the process noise with variance σ_w^2 ,

and the covariance of $P_w = I_{pxp}\sigma_v^2$. Both noise measurements $v(n)$ and $w(n)$ are mutually independent and uncorrelated.

$$x(n) = T(n-1)x(n-1) + w(n), \tag{3.4}$$

$$y(n) = C(n)x(n) + v(n), \tag{3.5}$$

where, $x(n) = [a_1(n), a_2(n), \dots, a_p n]^T$ is the unknown state vector; whereas the following matrix $T(n\text{-}1) = I_{pxp}$ is assumed to be an identity matrix, and $C(n) = [y(n-1), \dots, y(n-p)]$ is the observation data with discrete n-step. It is therefore important to know that the Kalman filter has mainly two processes, which are: time update or prediction, and measurement update or correction. At each step, the Kalman filter equations can be written as [65]:

$$x(n|n-1) = x(n-1|n-1) \tag{3.6a}$$

$$p_x(n|n-1) = p_x(n-1|n-1) + I\alpha_w^2 \tag{3.6b}$$

$$y(n|n-1) = C(n)x(n|n-1) \tag{3.7a}$$

$$\sigma_y^2(n|n-1) = C(n)\,p_x(n|n-1)C(n)^T + \sigma_v^2 \tag{3.7b}$$

and

$$k(n) = p_x(n|n-1)C(n)^T\,\sigma_y^2(n|n-1)^{-1} \tag{3.8a}$$

$$x(n|n) = x(n|n-1) + K(n)\left[y(n) - y(n|n-1)\right] \tag{3.8b}$$

$$p_x(n|n) = \left[1 - K(n)C(n)\right]p_x(n|n-1) \tag{3.8c}$$

where, $x(n|n\text{-}1)$ represents *a priori* estimate where its linear combination would result in $x(n|n)$, which is *a posteriori.* The Kalman gain, $k(n)$ would therefore give a weightage to the prediction error y(n|n) – y(n|n-1), so as to minimize the state estimation error x($n|n$); whereas $P_x(n|n\text{-}1)$, and $P_x(n|n)$ becomes the *priori* and *posteriori* error covariance estimates [65].

3.8. Damage Location Identification

For damage location, Sadhu and Hazra in [2] estimated the model shapes of the undamaged and damaged system to determine the damage location. The mode shape of the system under undamaged state can be utilized as a baseline data, and any difference in the mode shape ordinates under damaged state and the baseline data of the undamaged state can be used to find the damage location.

Mosavi et al. in [70] used a statistical measure called Mahalanobis distance to extract the damage features. This statistical measure recognize the variation patterns in the selected terms of the Vector Autoregressive (VAR) models by measuring the distance between the selected terms corresponding to a condition of interest, and the reference condition of the structure. Mahalanobis distances capture these deviations in the fitted VAR model coefficients, as the VAR extract the damage features for different sensor locations by measuring the amount of variations in the coefficients of VAR models obtained for a reference condition of the structure, and coefficients obtained for an unknown condition of the structure. Therefore, the selected terms of the fitted VAR models should experience the most extreme deviations at the sensor located closest to the physical damage location, as these coefficients are directly related to the model properties [70].

In this work, the damage localization is identified by taking the RMS percentage difference of the damage and the undamaged coefficients in each channel. Thus, the channel with the highest percentage difference is where the location closest to the physical damage location is.

3.9. Flowchart

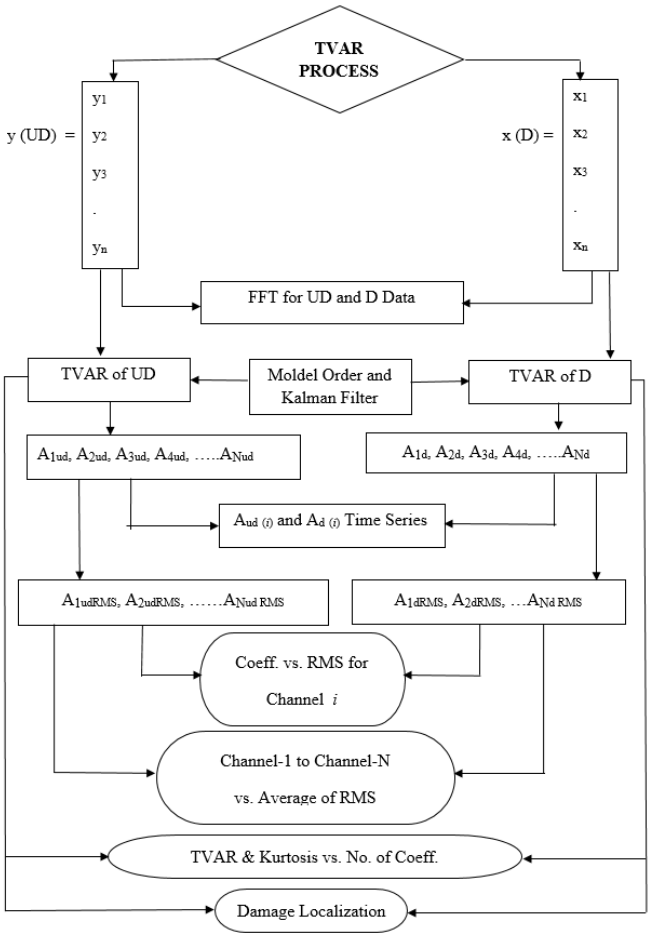

Figure 3.1: Flowchart

3.9.1. Description of Flowchart

Figure 3.1 shows the methodology flowchart representing the entire TVAR technique developed in this study, and supplemented with Kurtosis as per the following procedure:

(1) The undamaged (UD) data (y) with the damaged (D) data (x) are used as data inputs.

(2) FFT is then undertaken to observe the difference in the frequency and the amplitude between the UD and the D data, x and y.

(3) With model order carefully selected, and applying Kalman filter, the time series of the UD and D data is then created, followed by the plot of the Time Series for the UD and the D data.

(4) The model order is an important aspect for the creation of the AR model and the parameters defining the general structure of the model. Therefore, the coefficients which are realized by fitting the AR model appropriately to the data becomes the output of the model.

(5) RMS, a time-domain feature with the ability to measure the energy content of a signal and at the same time, contains signature of structural damage is created for all the channels.

(6) The RMS is plotted against coefficients for some selected channels.

(7) The developed TVAR technique is supplements with Kurtosis, which is likewise plotted against the number of coefficients to aid as an alternative technique for comparison purposes.

4. EXPERIMENTAL VALIDATION

4.1. Types of Models Used

The experimental validation comprises of two models: 6-DOF (model A), and a 5-DOF (model B), both developed at the LU Civil Engineering laboratory as shown in Figure 4.1. The experiments conducted on model A as shown in Figure 4.1 (a) and data collected is for the purpose of this work. Whereas for model B as shown in Figure 4.1 (b), it is developed during a degree project by LU Civil Engineering students whose data is acquired to be used for validating the technique developed. The reason why model B is used in addition to model A is because of the difference in the testing procedure conducted for both. While the bracing for model A was cut prior to running the test, the bracing for model B was cut when the test was running.

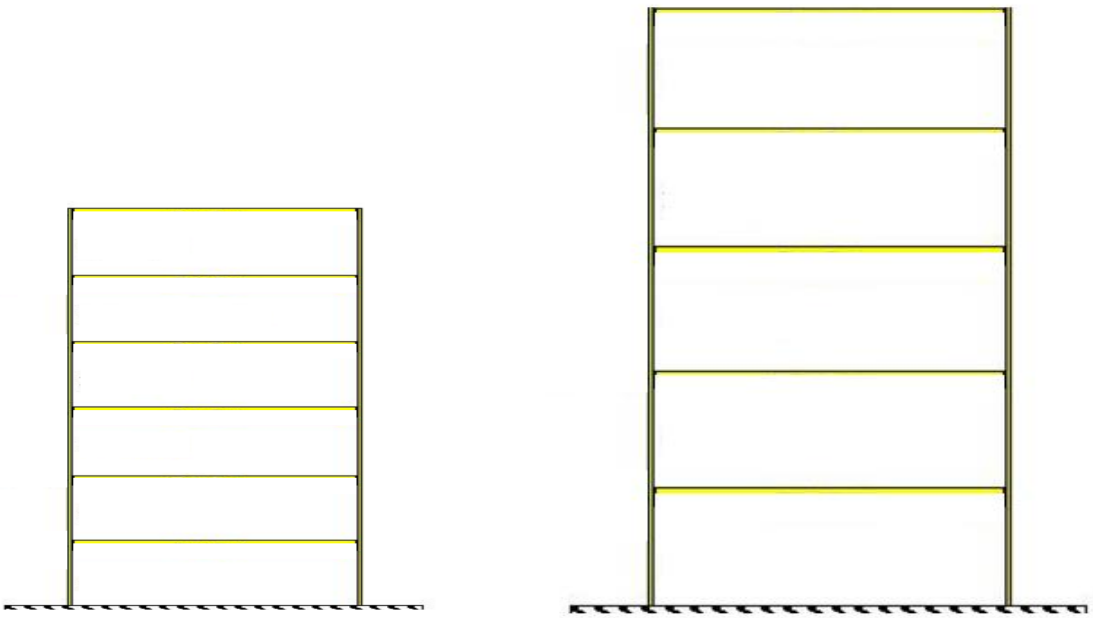

(a) Model A (b) Model B

Figure 4.1: Experimental models.

4.2. Fundamental Theory of Multiple Degree of Freedom System

As per Rao in [71], when any type of a system is allowed to vibrate freely after an initial disturbance, its frequency is the number of cycles of motion the system vibrates per second. However, with structural dynamics, a multi degree of freedom building needs to be reduced to

make the analysis simpler with reference to its frequencies, or when it is in free vibration (natural frequencies). Building floors are infinitely more rigid than the vertical columns, and therefore; the floors can be viewed as lumped masses. The joints of a building have only horizontal force, and therefore, the only mass to consider ideally is the floor weight.

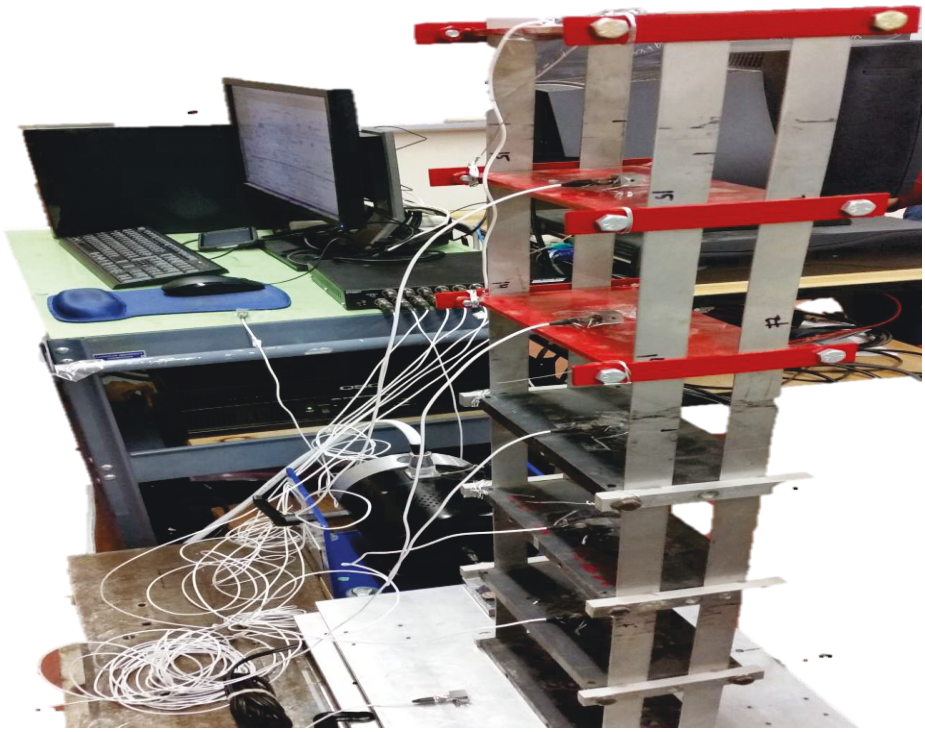

Figure 4.2: Model A.

4.3. Model A

4.3.1. Description

As shown in Figure 4.2, model A is comprised of steel plate on every story and bolted joints with two columns on each side. To create a dynamically excited load on the model and induce vibration, it is connected to a shaker which acts as a forced vibration source. The total mass of the model is determined to be 10.8 kg.

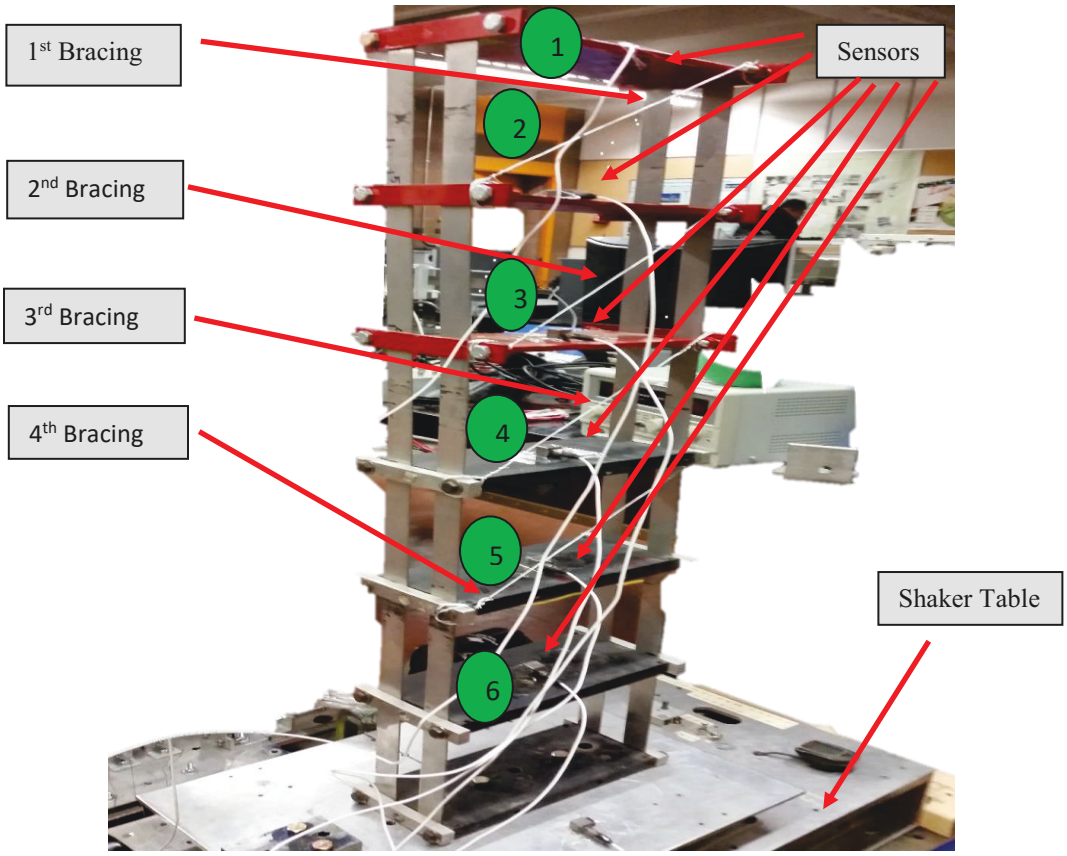

Figure 4.3: Model A with bracing.

4.3.2. Setup

Experimental setup of model A is shown in Figure 4.3. A wire as a bracing is used for only four floors starting from the top going downwards. A level is used to ensure that the mounted model is properly leveled on the shaker table. Thereafter, uni-axial sensors are attached starting from the top of the model floor, totaling up to six sensors attached to the model, one on each floor. The sensor on top of the floor represents Sensor-1, followed by Sensor-2 going downwards until Sensor-6. The sensors that were strategically placed on the model were used so as to accurately obtain the data when the model was undergoing vibrational excitation. The sensors locations are placed based on optimal sensor placement [74]. During testing, the sensors direct the data back to a dynamic signal acquisition system called QuickDAQ, where the data was processed on a desktop and exported for further analysis in MATLAB.

4.3.3. Experimental Procedure

The experiment was conducted through the following procedure. The model was attached to the shake table which provide random excitation in order to see all the structural modes. The sampling frequency of the data points used based on Nyquist– Shannon sampling theorem [15] was 200 Hz, and the procedure was performed as follows:

(a) Test-1: The first test was ran for 1 minute, then the shaking was stopped, and that represented the undamaged test with all the bracing intact.

(b) Test-2: As the apparatus was at rest, the first bracing on top was cut prior to the restart of the test, then the shaker was restarted, and likewise, Test-2 was recorded for another 1 minute, and that represented the first damaged test.

(c) Test-3: The same procedure was repeated as per Test-2 except that, it is the second from top bracing that was cut that represented the second damaged test.

(d) Test-4: This was done similar to Test-2 except that, it is the third from top bracing that was cut, and that represented the third damaged test.

(e) Test-5: This was again repeated as Test-2 except that, it is the fourth or the last from top bracing that was cut, and that represented the fourth or last damaged test.

In total, there were five tests conducted (one undamaged and four damaged tests). After the final test, the data files were saved for each test.

4.3.4. Data Analysis

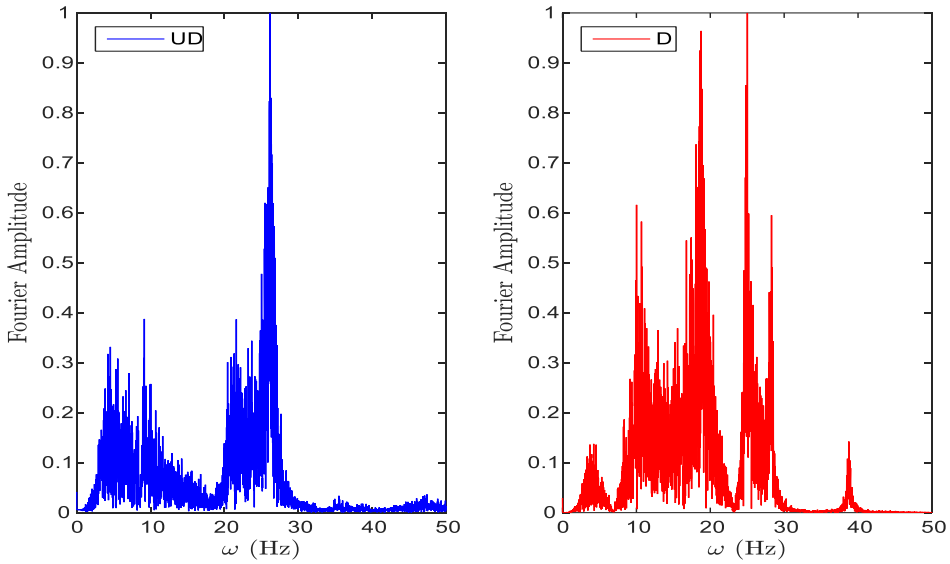

Figure 4.4: FFT of UD vs. D data for channel 4.

Table 4.1: Frequencies of UD and D data of model A.

Mode	ω (Hz)	Amplitude (UD)	ω (Hz)	Amplitude (D)
1	4.55	0.33	4.22	0.14
2	9.15	0.39	10.02	0.62
3	21.60	0.39	18.75	0.96
4	26.14	1.00	25.02	1.00
5	35.49	0.03	28.29	0.60
6	47.41	0.04	38.76	0.14

Using the experimental data with the sampling frequency of 200 Hz, the FFT for the undamaged (UD) and damaged (D) data is created. FFT generates corresponding displacement response spectra; hence, the natural frequencies and mode shape amplitude values were extracted from the displacement spectra of the undamaged and the damaged data using peak picking method [32]. With channel 4 being chosen because of its location which is not too flexible as the top of the floor or too rigid as the bottom, Figure 4.4 shows that the amplitude of Fourier spectra is higher for damaged FFT, an indication that the forced vibration induced by the shaker and the cutting of the braces have introduced some damage by reducing the structural stiffness. The damage is also

shown to be significant at the frequency of 28.29 Hz and 38.76 Hz as per table 4.1. On that other hand, the presence of damage in the structure causes changes in the frequency of the structure whereby the frequencies are mostly lower for the damaged than the undamaged frequencies.

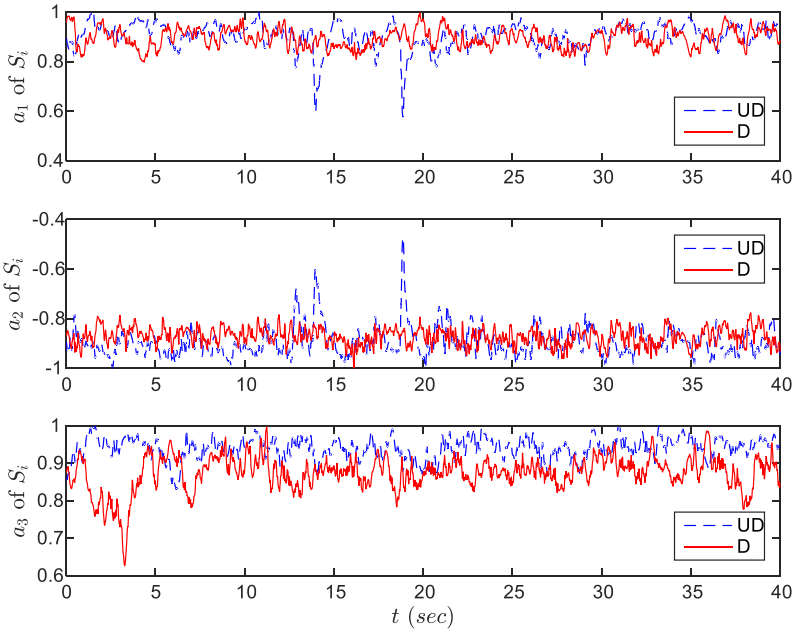

Figure 4.5: Coefficient a_1, a_2 and a_3 for the UD vs. D data of channel 1.

Since TVAR is sensitive to the choice of the model order, it therefore requires the right selection, as inappropriate model order only results in model parameters that will not characterize the underlying nature of the process, thereby, resulting in an inaccurate representation of the signal. To further establish the TVAR model, the smoothness constant which in this case is the Kalmen filter is applied. This is done in order to normalize the amplitude automatically inside the function so that the amplitude of the entire signal will be adjusted to have a maximum value of 1. Thus, for the time series result of model A shown in Figure 4.5, the model order of 18 is chosen, and the coefficient of a_1, a_2 and a_3 for the undamaged versus damaged data shows that the damaged time series is more fluctuated, an indication of the effects of excitation and the damage induced as a result of cutting of the braces. Subsequent results are in the following Figures.

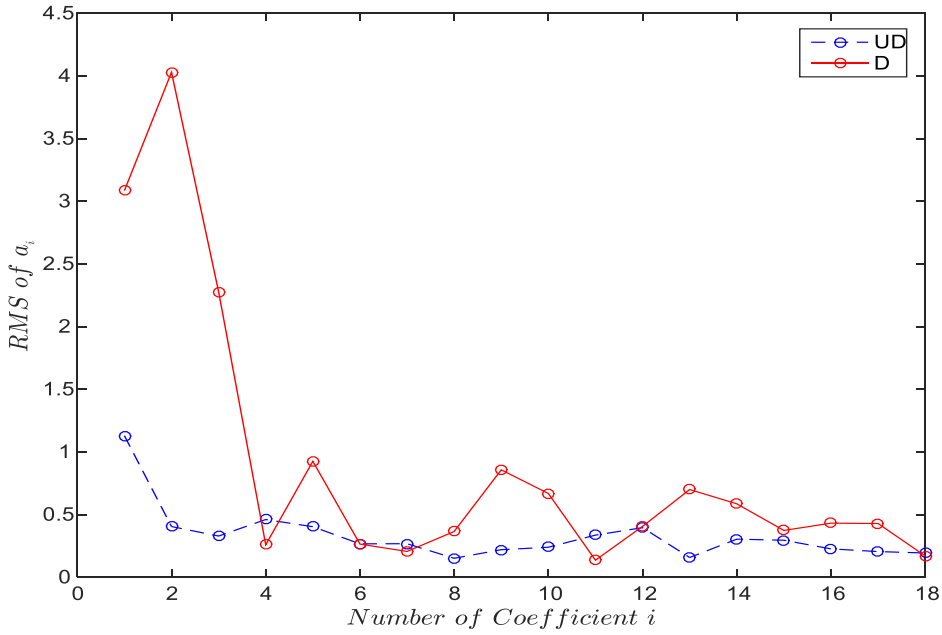

Figure 4.6: RMS values of TVAR coefficients of channel-1 using model order of 18.

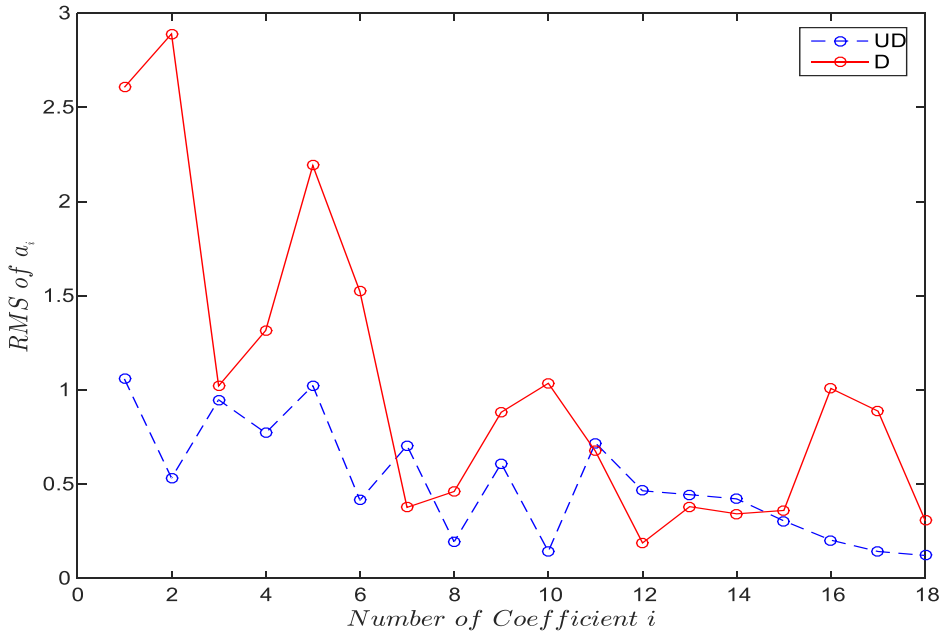

Figure 4.7: RMS values of TVAR coefficients of channel-2 using model order of 18.

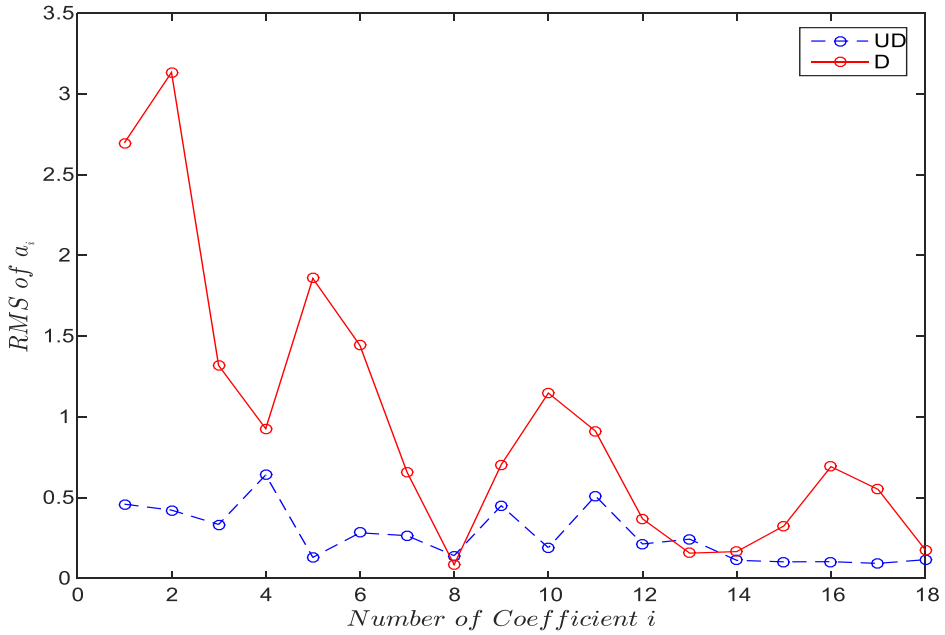

Figure 4.8: RMS values of TVAR coefficients of channel-3 using model order of 18.

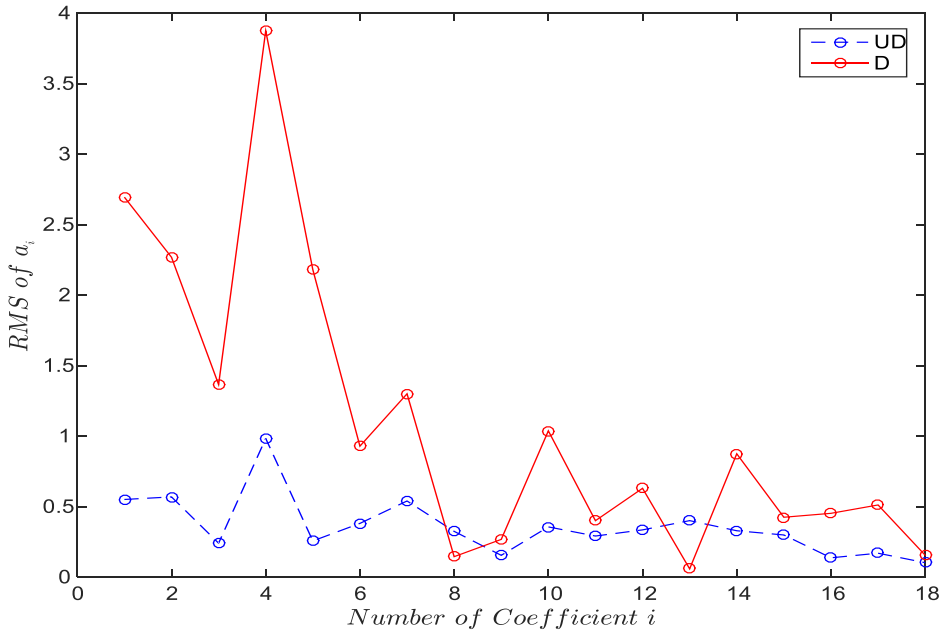

Figure 4.9: RMS values of TVAR coefficients of channel-4 using model order of 18.

After selection of the right model order 18, results of time series of channels a_1, a_2 and a_3 were obtained. Kalman filter is then applied for the normalization of data, and the RMS for all channels were created and plotted versus their coefficients as shown in Figures 4.6, 4.7, 4.8, 4.9, 4.10 and 4.11. Hence, the following is the observation of the model performance:

- For channel 1 (Figure 4.6), coefficients a_1 and a_2 are showing the biggest RMS difference as indications of damage.
- Same for channel 2 (Figure 4.7) whereby, coefficients a_1 and a_2 are also showing the RMS biggest difference.
- As for channel 3 and 4 (Figures 4.8 and 4.9), damage were detected in all the coefficients with the exception of coefficients 8 and 13.
- With channel 5 (Figure 4.10), damage were also detected in all the coefficients except in coefficients 10, 11 and 12.
- Whereas for channel 6 (Figure 4.11), some damage were detected in all the coefficients except in coefficients 3, 8, 16 and 17.

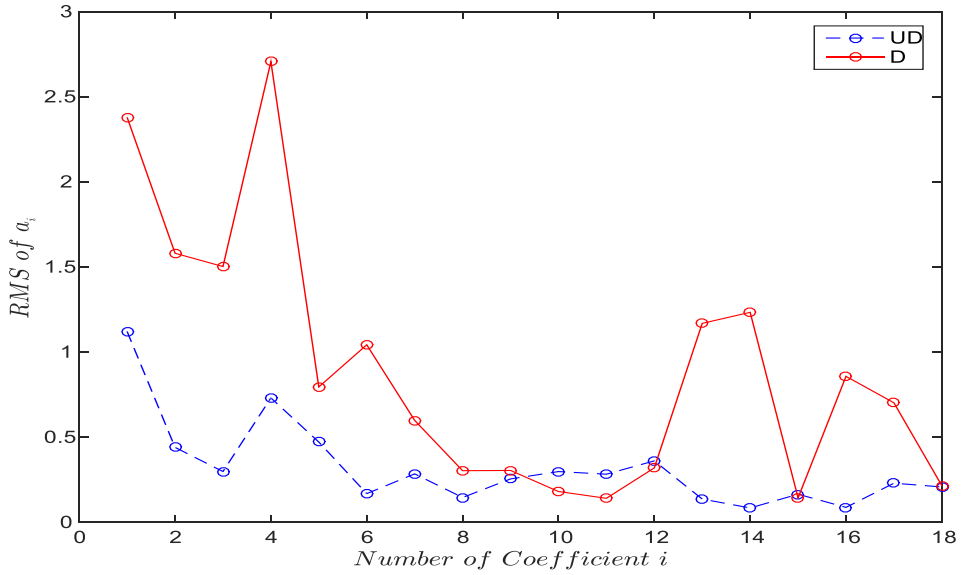

Figure 4.10: RMS values of TVAR coefficients of channel-5 using model order of 18.

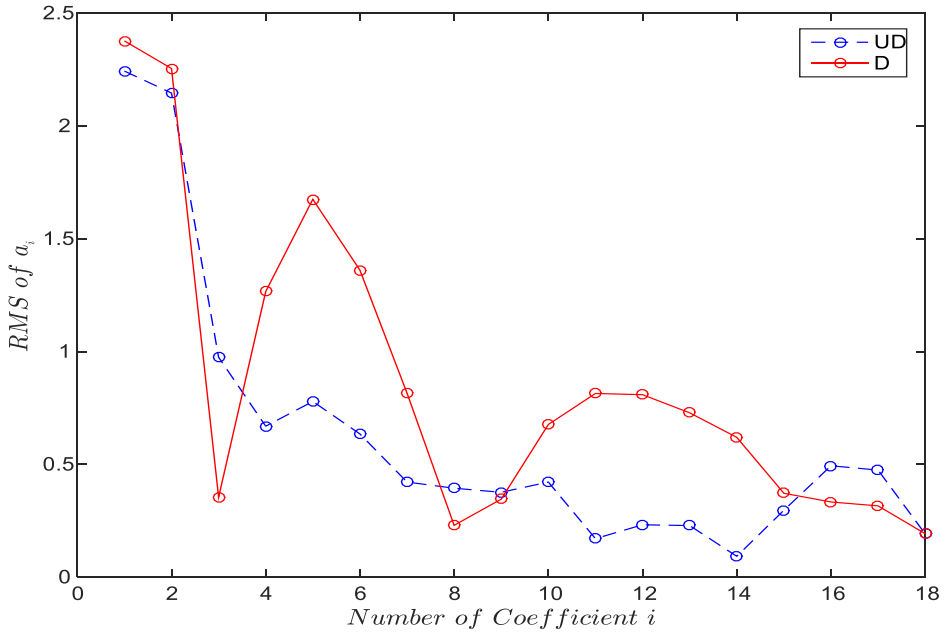

Figure 4.11: RMS values of TVAR coefficients of channel-6 using model order of 18.

4.3.5. RMS vs. Kurtosis

Subsequent to applying the TVAR technique and obtaining the results for all the six channels, for comparison purposes, TVAR is supplemented with Kurtosis. By definition, Kurtosis is the measure of peakedness of distributions, and therefore, a distribution with kurtosis higher than 3 is referred to as Leptokurtic, and when the kurtosis less than 3 is Platykurtic; whereas for the Gaussian distribution, the kurtosis is 3 and is called Mesokurtic. In a nutshell, Kurtosis greater than 3 indicates more data far from the mean or some peaks can be observed in the data distribution. If the kurtosis is less than 3, the data distribution is flat with short tails. With Kurtosis which can also be utilized as an important feature in representing fault condition, it is applied to channel 5 as per Figure 4.12.

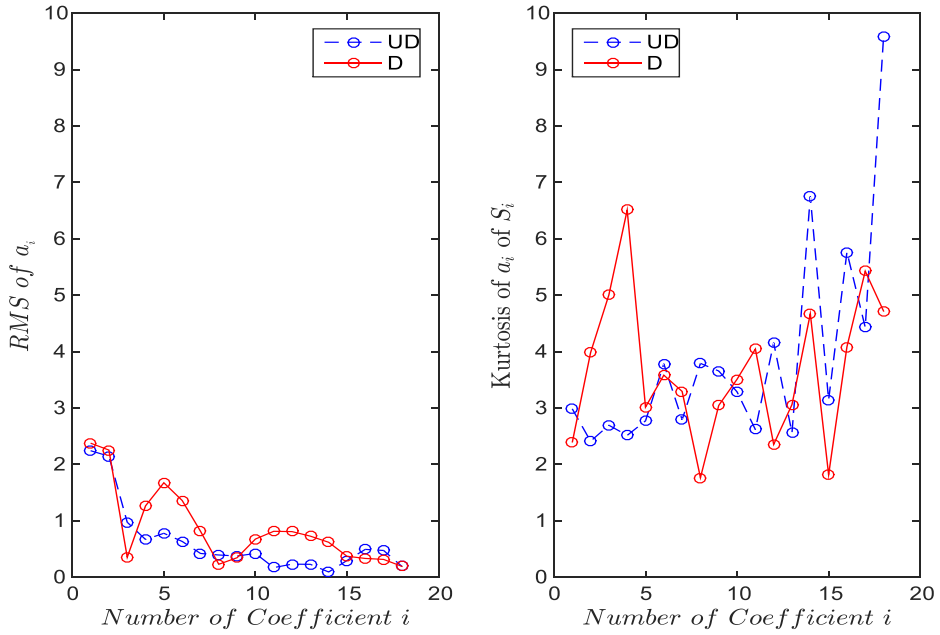

Figure 4.12: Comparison of the RMS values of TVAR coefficients of channel-5 using model order of 18 with Kurtosis of S_i.

Since Kalman filter have been applied to TVAR, under the same condition, Kurtosis results for the undamaged data shows that it is higher than 3, which means Leptokurtic for the following coefficients: 6, 8, 9, 10, 12, 14, 16, 17 and 18. For the damaged case, Kurtosis is Leptokurtic as expected in the following coefficients: 2, 3, 4, 6, 7, 10, 11, 14, 16, 17 and 18. In overall, Kurtosis is more leptokurtic for the damaged case, an indication of the presence of damage due to the excitation of the structure and the cutting of the braces. As for the Kurtosis coefficients less than 3 or Platykurtic, out of the undamaged coefficients, there are more coefficients with Kurtosis that are Platykurtic. Whereas for the damaged case, there are less coefficients with Kurtosis that are Platykurtic, an additional indication that more damage is detected.

With the six channels plotted in Figures 4.6, 4.7, 4.8, 4.9, 4.10 and 4.11, the coefficients are showing the biggest RMS difference in a_1 and a_2, and that is why a_1 and a_2 are chosen and plotted for all the channels in order to observe the performance of the model.

Therefore, results are shown in Figures 4.13 for coefficient a_1 and 4.14 for coefficient a_2. Figure 4.13 shows higher damage in channel 1, but damage is reduced in the subsequent channels due to

the locations of the channels close to the base which is more rigid compared to the top of the model. Whereas for Figure 4.14 for coefficient a_2, damage is also significant in channel 1, but reduced in the rest of the channels. Since the biggest RMS difference is in channel 1 for coefficient a_2, it is for this reason that it is further considered for damage localization as per Figure 4.15.

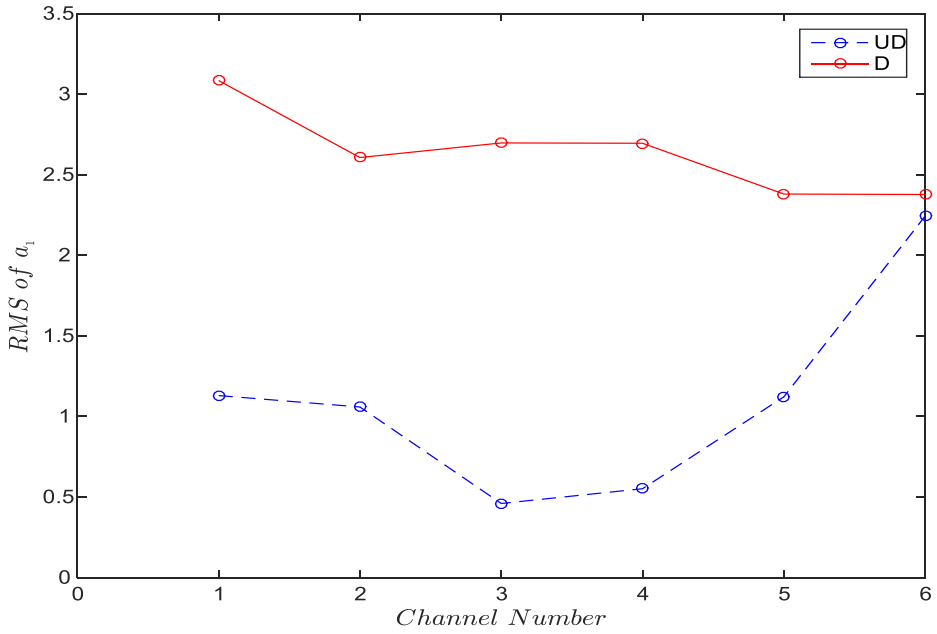

Figure 4.13: RMS values of TVAR coefficients a_1 using model order of 18.

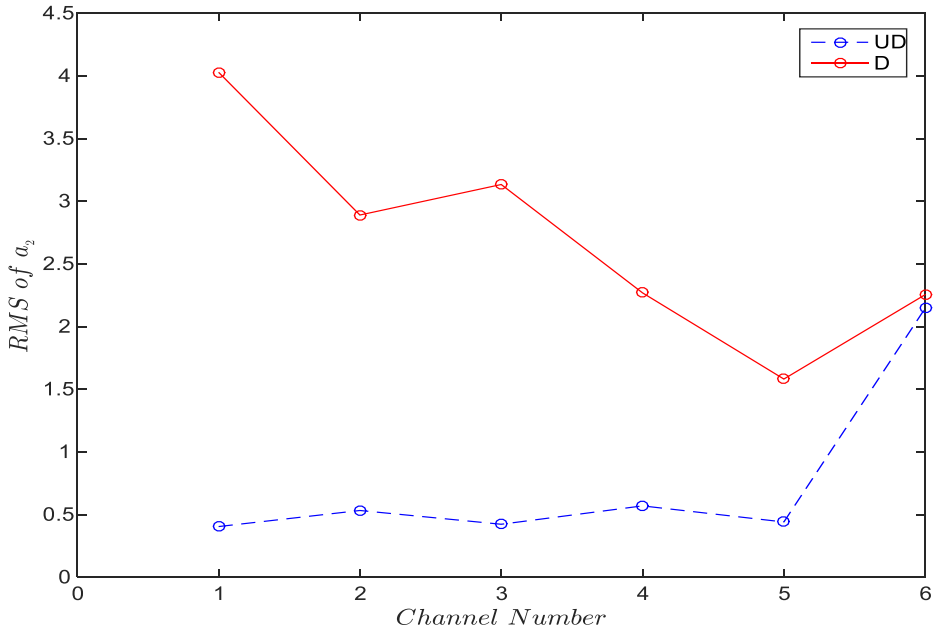

Figure 4.14: RMS values of TVAR coefficients a_2 using model order of 18.

For damage localization as shown in Figure 4.15, RMS percentage difference in the energies of the signal of the damage and the undamaged data are considered and calculated. Where the highest RMS is, its corresponding channels should be where the damage is located. Thus for model A, the damage is located in channel 1 and 3, but less in channels 4, 5 and 6 due to the rigidity of the structure. As for channel 2, issues that might have contributed to it being less might be the location of the sensor or its placement on the structure.

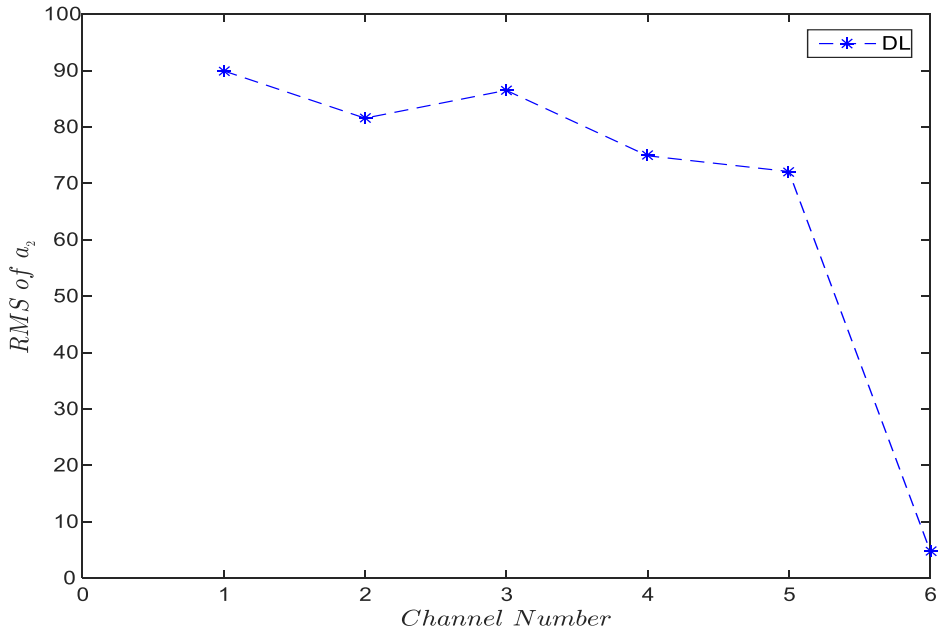

Figure 4.15: RMS percentage difference of TVAR coefficient a_1 for damage localization.

4.3.6. Conclusion

Results shows that the AR model and parameters which define the general model structure, plus the coefficients which are realized by fitting the AR model to the data have allowed the model to infer with the dynamics of the data. That is how damage detection and localization is achieved.

4.4. Model B

4.4.1. Description

The model was a 10 DOF fabricated and welded structure, designed for the purposes of SHM studies under Dr. Ayan Sadhu at the Lakehead University department of Civil Engineering. It comprised of four columns of steel tubes with plates on each story welded onto the columns.

4.4.2. Description of all experiments

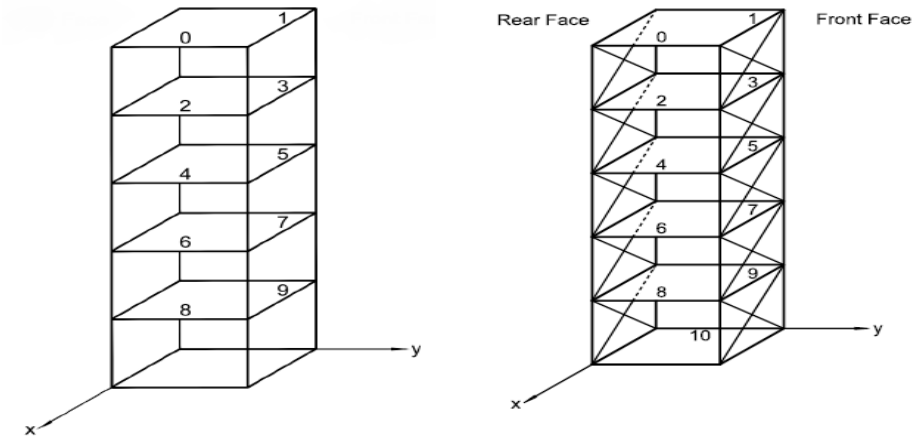

(a) Free vibration (b) Forced vibration with braces

Figure 4.16: Model B vibration testing.

4.4.3. Model B Testing Set-up

A partial layout of the experiments conducted on the structural model is shown in Figure 4.17, with the sensor locations and labels of the sensors being indicated by numbers in Figure 4.16 (a) and (b). Whereas table 4.2 shows the descriptions of all the experiments performed. Some of the tests conducted were symmetrical about the x and y axis, hence, one direction is only shown.

Figure 4.17: Braced structure resting on top of the shaker table.

4.5. Experimental Procedure of Model B

For the vibration testing, wires used as braces were hand tightened on to the model as per Figure 4.17. Free vibration tests were then conducted, thereafter, the damage tests were performed as follows:

(a) The model was randomly shaked for 5 seconds.

(b) Data was then collected for 10 seconds.

(c) The bracing was immediately cut after the 10 seconds.

(d) Data collection was continued for another 10 seconds.

(e) Data collection and random shaking were then stopped.

(f) Test restarted and the bracing of the structural model were then cut during tests 20 through 29.

4.5.1. Braced Vibration Testing Descriptions

Table 4.2: Summary of vibration testing of building model with bracing.

Excitation Description	Bracing
Random Shaking	All Floors Braced
Random Shaking	Front face brace on Top floor cut mid test
Random Shaking	Rear face brace on Top Floor cut mid test
Random Shaking	Front face brace on 4th floor cut mid test
Random Shaking	Rear face brace on 4th Floor cut mid test
Random Shaking	Front face brace on 3rd Floor cut mid test
Random Shaking	Rear face brace on 3rd Floor cut mid test
Random Shaking	Front face brace on 2nd Floor cut mid test
Random Shaking	Rear face brace on 2nd Floor cut mid test
Random Shaking	Front face brace on 1st Floor cut mid test
Random Shaking	Rear face brace on 1st Floor cut mid test

For data collection, the sampling frequency of the data points was set to 200 Hz. With the accelerometer placed to detect the accelerations felt on each floor, motions are relayed into a computer, and a text file is created which contains data points of acceleration and timestamp.

4.5.2. Results

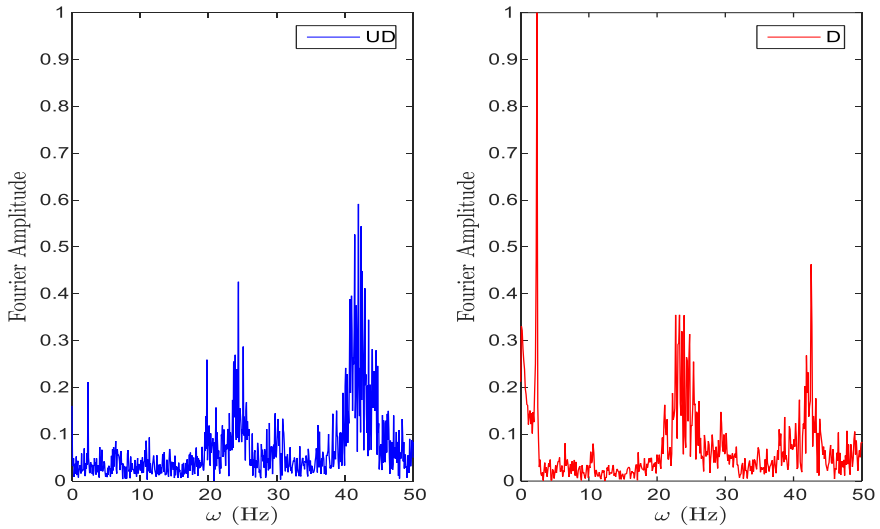

Figure 4.18: FFT of UD vs. D data for Channel 4.

Table 4.3: Frequencies of UD and D data of Model B.

Mode	ω (Hz)	Amplitude (UD)	ω (Hz)	Amplitude (D)
1	2.346	0.211	2.397	1.000
2	11.340	0.093	6.507	0.081
3	19.780	0.259	10.620	0.080
4	24.390	0.426	17.240	0.061
5	29.790	0.145	23.390	0.354
6	46.360	0.150	42.580	0.463

Whereas for Figure 4.18 for model B, likewise, the sampling frequency of 200 Hz were used for channel 4 to create the FFT for the UD and D data. As a result, the FFT shows higher Fourier amplitude in almost all the six modes, with significant damage at 42.580 Hz which is lower than the UD frequency of 46.360 Hz as per table 4.3.

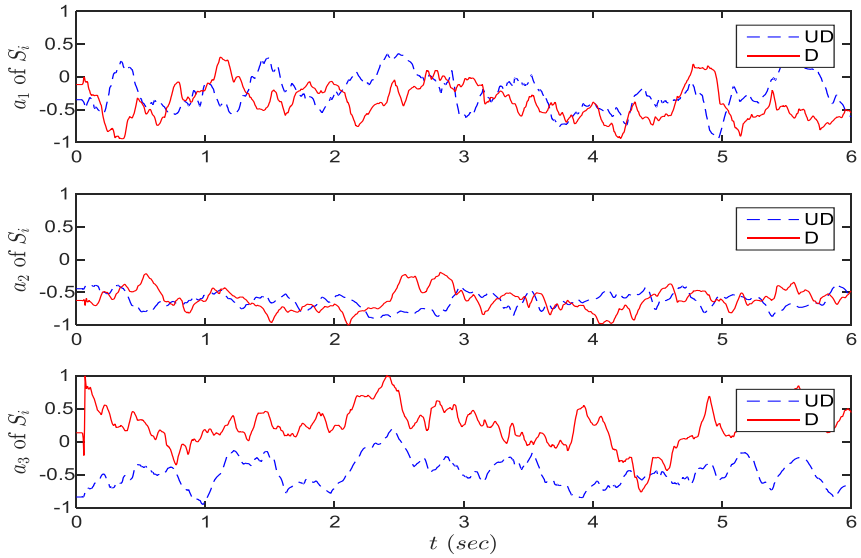

Figure 4.19: Coefficient a_1, a_2 and a_3 for the UD vs. D data of channel 7.

The time series result of model B in Figure 4.19 shows more fluctuations in the D than the D. Unlike the model order 18 which worked best for model A, it is model order 16 which is chosen for model B, and the way the order is chosen is illustrated in the below section 4.5.3.

4.5.3. Illustration of how the Model Order is Chosen

In selection of the model order, RMS values for each coefficients under undamaged and damaged case are determined as the time-domain features to measure the changes in the energy content of the signal. The RMS values are then observed as model order are applied until the optimal model order is identified using trial and error method. This practice is shown in Figure 4.20 versus 4.23 using channel 11 to observe the differences in order to choose the best fitted model.

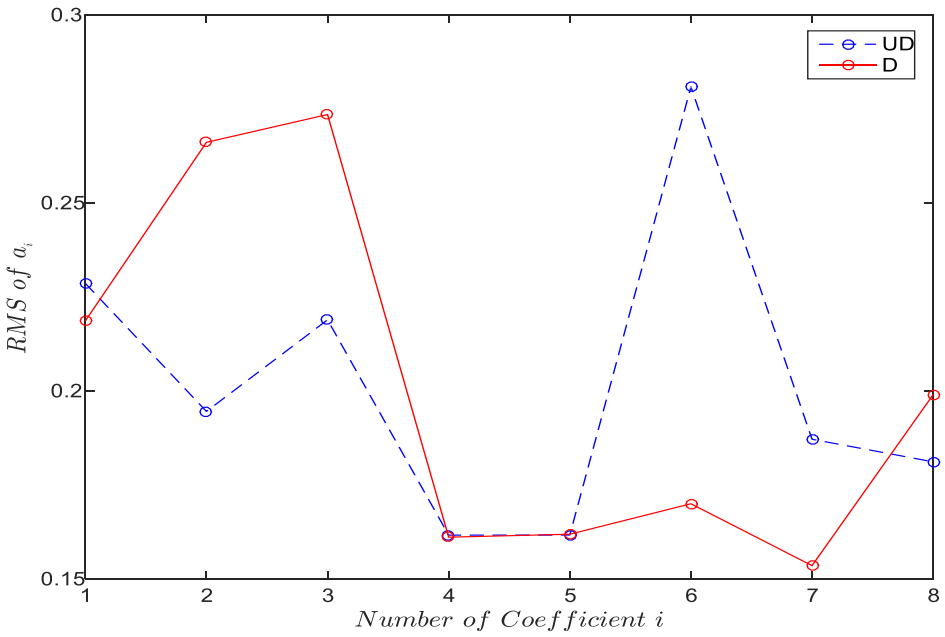

Figure 4.20: RMS values of TVAR coefficients of channel-11 using model order of 8.

Using channel 11 as a benchmark, the choice of model order 8 is disregarded due to the fact that it didn't fit the model as shown in Figure 4.20 where damage is not detected very well. Whereas for Figure 4.23, model order 16 became the best fit as the observation of the RMS versus coefficients shows some indications of damage in all the coefficients. This allows the model to be further analyzed with the right choice of the model order 16.

The application of TVAR provide the resulting Figures 4.21 and 4.22 which shows that, the model is capable of detecting damage as being reflected in almost all the coefficients. The only exception is that, in coefficient 12 for Figure 4.21, it shows slightly higher undamaged RMS and lower damage RMS. Whereas for Figure 4.22, there are more damage coefficients with higher RMS. In Figure 4.23, RMS values is higher for all the damaged coefficients. For the sake of comparison, Kurtosis is applied to channel 4 as per Figure 4.24.

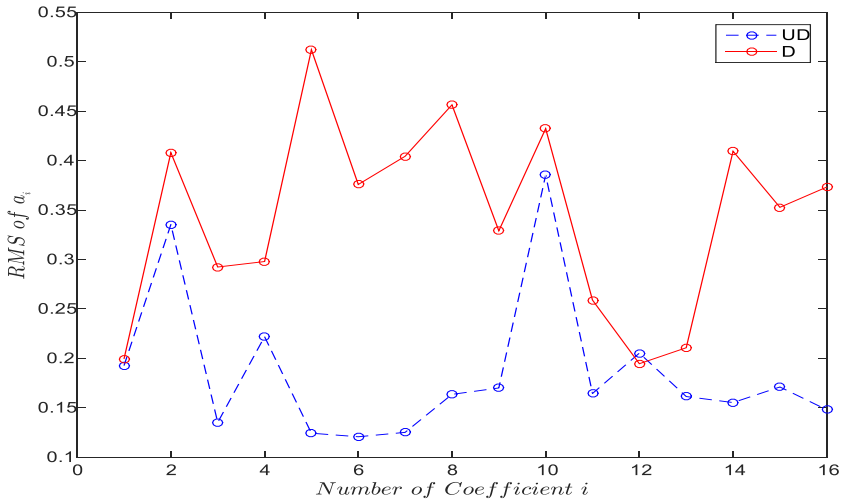

Figure 4.21: RMS values of TVAR coefficients of channel-4 using model order of 16.

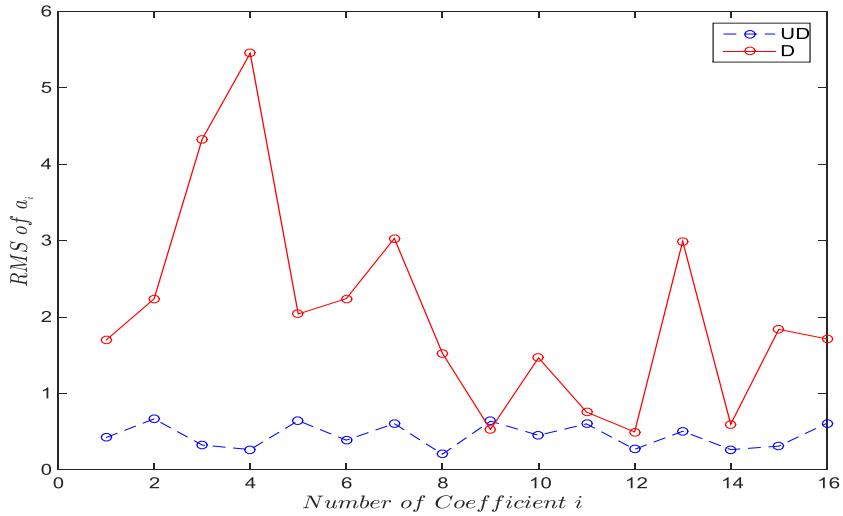

Figure 4.22: RMS values of TVAR coefficients of channel-5 using model order 16.

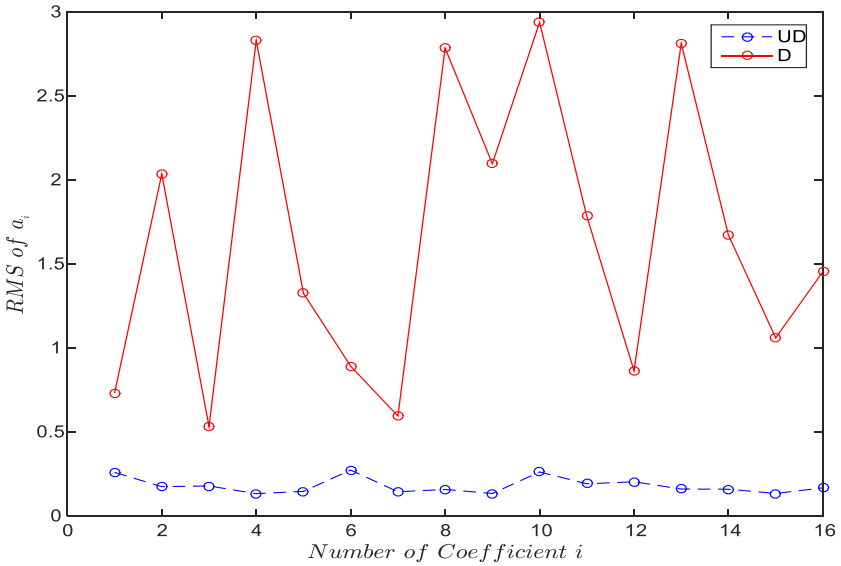

Figure 4.23: RMS values of TVAR coefficients of channel-11 using model order of 16.

4.5.4. RMS vs. Kurtosis

Result on Figure 4.24 shows that for the undamaged case, Kurtosis is Leptokurtic (higher than 3) for the following coefficients: 2, 3, 7 and 12. For damaged case, it is Leptokurtic in coefficients 2, 4, 6, 7, 8, 10 and 14, which means more Leptokurtic Kurtosis in the damaged coefficients than the undamaged coefficients. In overall, out of the 16 coefficients, there are less Kurtosis that are Platykurtic in the damage coefficients, a sign that Kurtosis is similarly capable of detecting damage in model B.

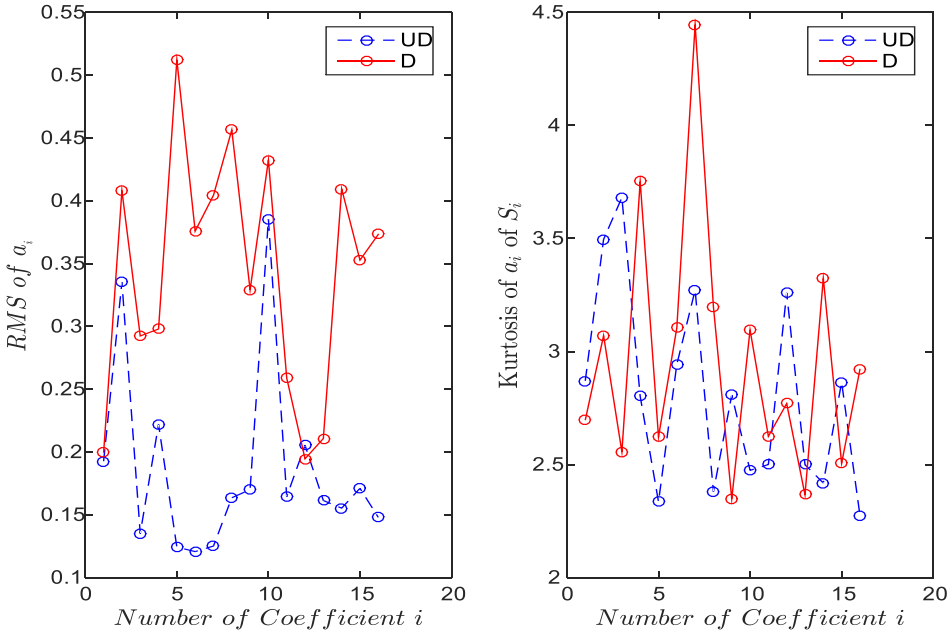

Figure 4.24: Comparison of the RMS values of TVAR coefficients of channel-4 using model order of 16 with Kurtosis of S_i

Subsequent approach for model B is to average all the 12 channels using TVAR so as to further analyze the model accordingly. The RMS average of all the channels and their corresponding coefficients is shown in Figure 4.25. The average of RMS values of a_i versus channel number in Figure 4.25 shows that the model is best fitted. Channel 4 shows 0.578 undamaged RMS and 0.344 damaged RMS. For channel 8, it shows 0.576 undamaged RMS and 0.204 damaged RMS. In overall, the performance of the model indicates that there are more damage channels being observed than the two undamaged channels 4 and 8 with little higher RMS.

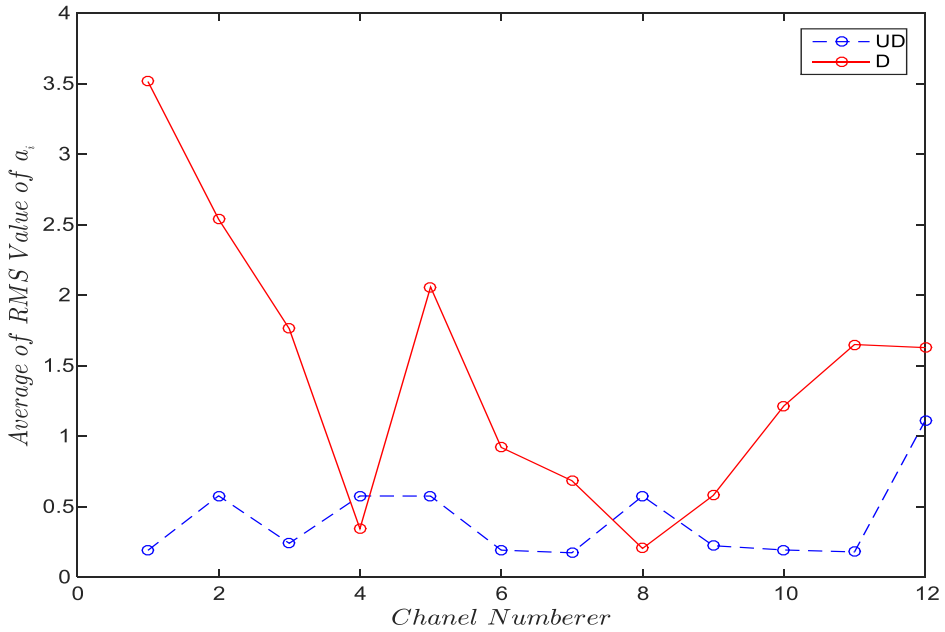

Figure 4.25: Average of RMS value of a_i vs. channel number using model order of 16.

Since coefficient a_1 and a_2 are showing the biggest difference in terms of higher RMS, a_1 and a_2 will be plotted for all the different channels. This is shown in Figures 4.26 for coefficient a_1 and 4.27 for coefficient a_2.

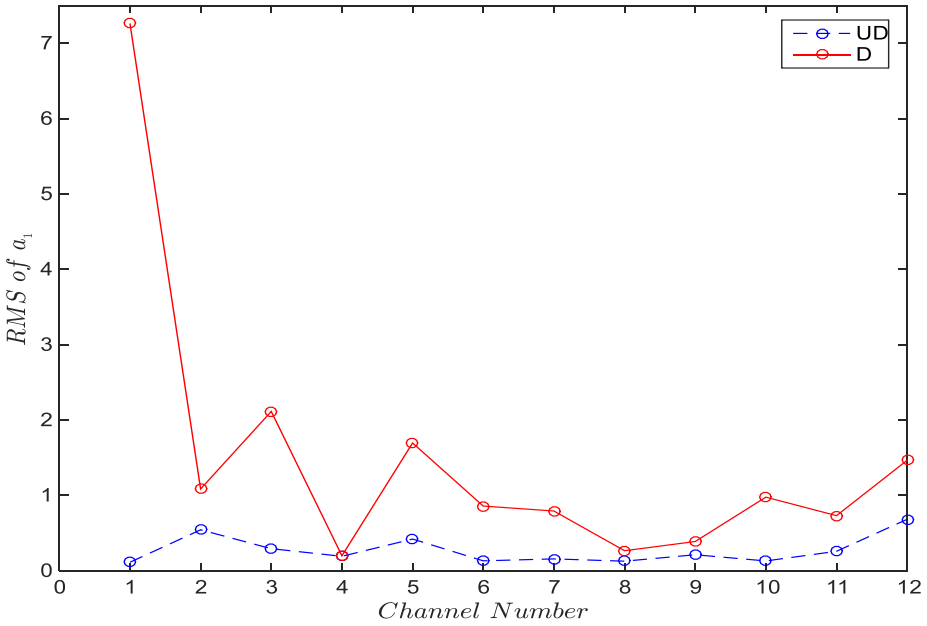

Figure 4.26: RMS values of TVAR coefficients a_1 using model order of 16.

Both Figures 4.26 and 4.27 shows that, the coefficient of channel 1 has the highest RMS. That leads to the identification of the damage whereby, RMS percentage difference in the energies of the signal of the damage and the undamaged data is calculated with the results shown in Figure 4.28 which shows that damage is highest in channel 1

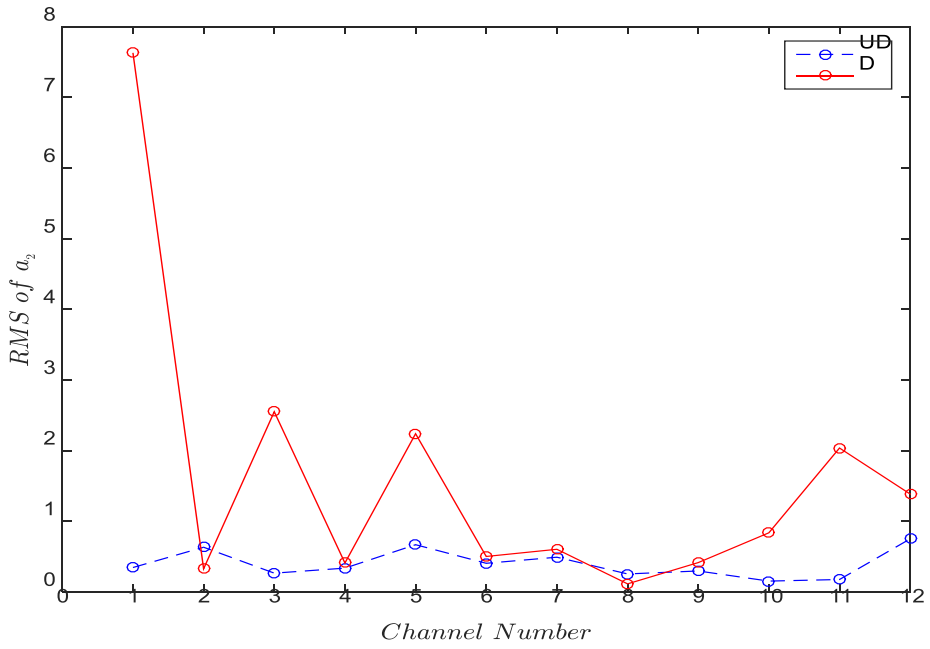

Figure 4.27: RMS values of TVAR coefficients a_2 using model order of 16.

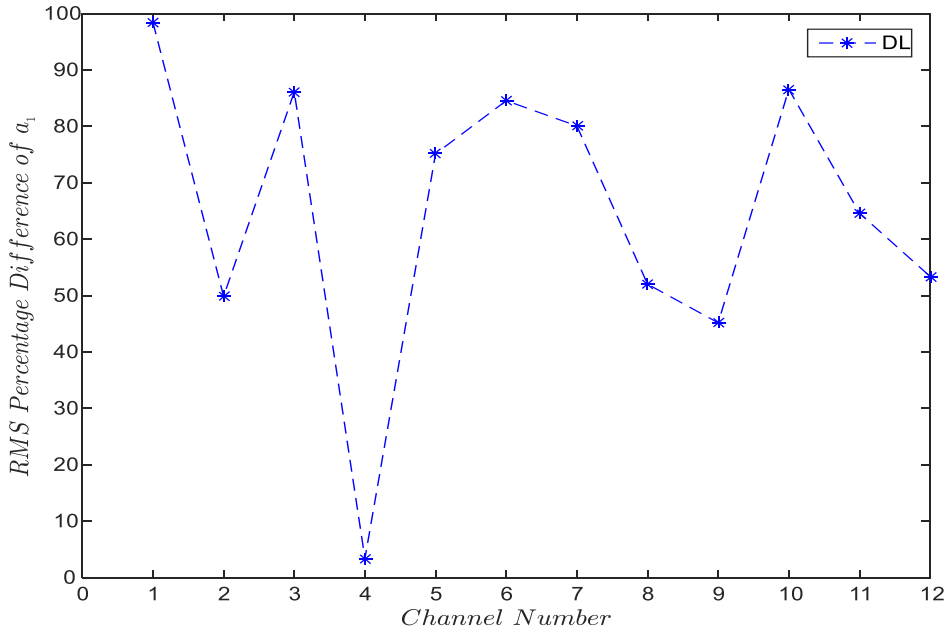

Figure 4.28: RMS percentage difference of TVAR coefficient a_1 for damage localization.

4.5.5. Conclusion

The model performance shows that it is capable of damage detection and localization. Damage localization appeared in channel 1 because the top of the floor level is prone to more vibration as opposed to the base of the floor which is rigid because of its attachment to the base. On the other hand, channel 4 seems to have exhibit less damage and that might be due to factors such as the location of the sensor, placement or more structural stiffness where the sensor is placed.

5. FULL SCALE VALIDATION

5.1. Description

The data obtained is from an actual cable-stayed bridge with an implemented SHM system [72], which monitors vehicle loads, cable stresses, girder strains, accelerations, wind, temperature, and humidity, employed as the benchmark structure by HIT. The bridge which is shown in Figure 5.1, is one of the first cable-stayed bridges constructed in mainland China [73, 74]. The bridge consists of a main span of 260 meters (m), and two side spans of 25.15 + 99.85 meters each. The length of the bridge is 510 meters long and 11 meters wide, which comprised of 9 meters for the vehicles and 2 x 1 meters for the pedestrians. The concrete bridge tower consist of two transverse beams, which is 60.5 meters tall, and was constructed using sliding formwork technology. The main girder was assembled from 74 precast concrete girder segments, formed continuously by cast-in-place joints that connect the girder ends and form transversely reinforced diaphragms [73, 74].

The 2 x 41.6-meters prestressed girder of the side span was built on the site using formwork supported by temporary false work. There are a total of 88 pairs of cables containing steel wires, which is 5 millimeters in diameter. The minimum number of steel wires within a cable is 69 and the maximum is 199. The design cable tension forces under dead load range from 559.4 to 1,706.8 Kilo-Newton (kN), and the stress is approximately 450 Mega pascal (MPa); whereas the design stress in the cables due to live load is 160 MPa. The construction of the bridge started in 1983, and it became operational to traffic in December 1987 [73, 74].

After 19 years of operation, cracks with a maximum width of 2 centimeter (cm) were observed at the bottom of a girder segment over the mid-span, and these cracks may have been induced by overweight vehicles, as the weights and the volumes of vehicles on the bridge are much greater than anticipated in the original design. The stay cables, especially those near the anchors

were severely corroded and repairs were conducted between 2005 and 2007 where the girder over the mid-span was recasted, and all of the stay cables were replaced [73, 74].

Figure 5.1: General view of the investigated bridge [73].

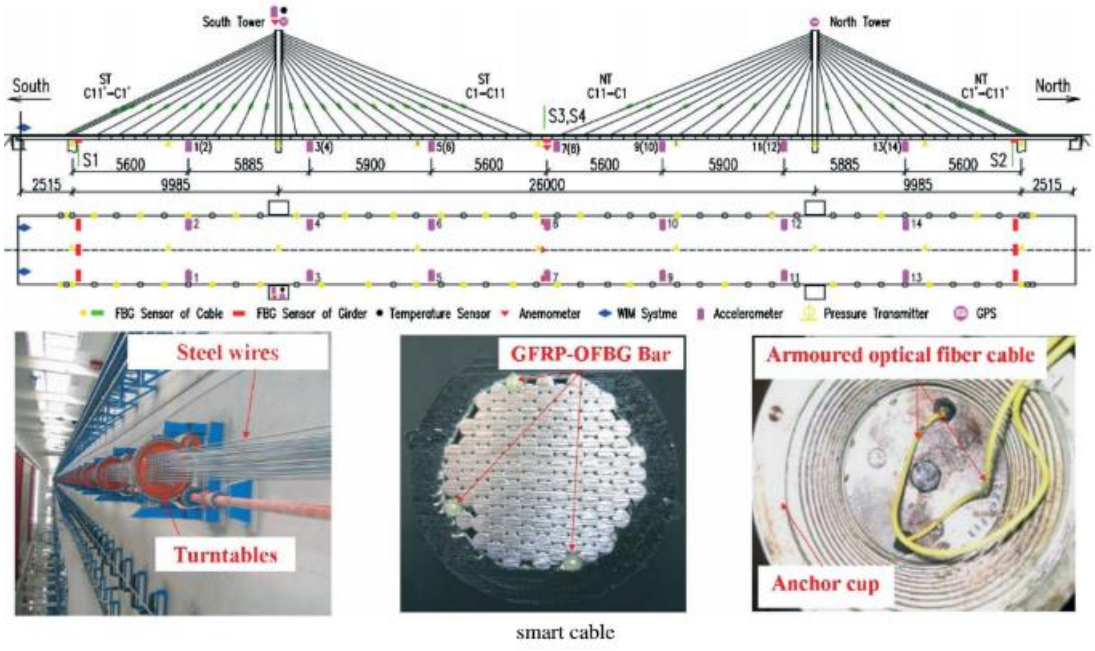

Figure 5.2: Sensor setting and smart cable embedded with OFBG sensors of SHM system [73].

5.2. Full Scale SHM Established System

During the repair and rehabilitation process, a sophisticated SHM system was designed for the bridge and implemented by the Center of SMC at HIT [72]. A diagram of the SHM system is shown in Figure 5.2. As part of the SHM system, more than 150 sensors were installed on the bridge's cables, towers, and girders, and data acquisition devices were located in the control room. Fourteen uniaxial accelerometers were permanently installed on the deck, and one biaxial accelerometer was attached to the top of the south tower so as to monitor the horizontal oscillation of the tower [73, 74].

An anemoscope and a temperature sensor were also attached to the top of the south tower to measure the 3-D wind velocity and ambient temperature respectively. A WIM system was mounted on the bridge deck for all lanes, and Optical Fiber Bragg Grating (OFBG) sensors were embedded into the newly cast concrete, or welded onto the girder - the existing concrete, for strain and temperature measurement at some critical locations which is S1–S4 as shown in Figure 5.2 (top Figure) [73, 74].

In the study by HIT, smart cables with embedded OFBG sensors shown in Figure 5.2 (bottom Figure) were employed in the SHM system so as to record the time history of the cables' stresses. Peripheral Component Interconnect Based Techniques and a LabVIEW-based acquisition program were employed for data collection. A wireless Motorola instrument was installed on top of the south tower to transmit data from the personal computer on the bridge site to the server at the toll station - with 2 MB of information at a time transmitted across 15 km. Thereafter, all the measured data from the sensors and structural information were saved and managed in an SQL Server 2000 database on the main server. Li et al. in [75] provided the detailed information on the SHM system including the DAQ system and the data transmission system.

5.3. Description of data

The following information is from the data manual which addressed the data contained in the online database, controlled by the HIT [72]. Based on the study, the acceleration and environmental conditions collected by the SHM system were done in the following months: January 1, January 17, February 3, March 19, March 30, April 9, May 5, May 18, May 31, June 7, June 16 and July 31, 2008. These were selected as the benchmark time history of the bridge, from a healthy status to a damaged one [74].

While considering the effects of temperature and the wind velocity might have certain impacts on model parameters of cable-stayed bridges [72], the environmental conditions of the corresponding accelerations were also reported in the study. For the acceleration data, there are a total of 17 columns. In each file, the first column represents the measurement time and the next 16 columns denote the acceleration time history, which were collected using 14 uniaxial accelerometers that had been installed on the bridge deck, and 1 biaxial accelerometer affixed on the top of south tower. The sampling frequency of the acceleration is 100 Hz [74].

5.4. Field Testing

For the field testing acceleration, there are a total of 18 accelerometers which were used to measure the semi-span acceleration of the upriver or downriver lanes each time. The 1st to 18th accelerometers were located from the side span to the mid-span, which is labeled as 1 through 18 at the south tower side, or 1' through 18' at the north tower side as per Figure 5.3.

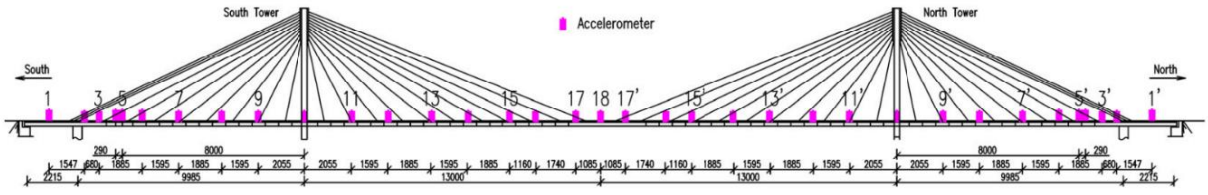

Figure 5.3: Accelerometer location in the field testing [75].

The locations on the south tower side and the north tower side were symmetrical. The reference sensor selected was Accelerometer 18 as modeled by HIT. As for the vibration field testing [72, 74], it was conducted four times, once each day from the 7th to the 10th of August 2008. The acceleration files were described as follows according to the data manual:

(1) Filename ACC08-8-7: Semi-span of downriver acceleration on the south tower side, measured on August 7, 2008 with a 32 Hz sampling frequency.

(2) Filename ACC08-8-8: Semi-span of downriver acceleration on the north tower side, measured on August 8, 2008 with a 20 Hz sampling frequency.

(3) Filename ACC08-8-9: Semi-span of upriver acceleration on the north tower side, measured on August 9, 2008 with a 20 Hz sampling frequency.

(4) Filename ACC08-8-10: Semi-span of upriver acceleration on the south tower side, measured on August 10, 2008 with a 20 Hz sampling frequency.

Each file has its own file heading which included the beginning and ending time of testing, sampling frequency, actual sensitivity (V/g) and the channel number. In accordance to the structure of the data collected, there were a total of 36 columns in each file, whereby, 18 accelerometers were used each time. The odd number columns give the time while the even number columns were the acceleration measurements (V).

5.5. Results of full-scale data

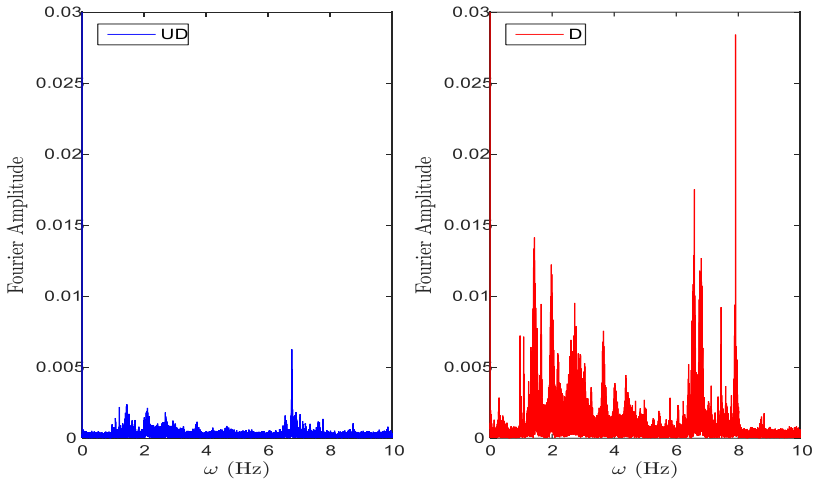

Figure 5.4: FFT of UD – Jan Data vs. D - May data for channel 16.

Table 4.4: Frequencies of UD and D full scale HIT data.

Mode	ω (Hz)	Amplitude (UD)	ω (Hz)	Amplitude (D)
1	1.4430	0.0024	1.4290	0.0141
2	2.1080	0.0021	1.9730	0.0122
3	3.7070	0.0012	2.7230	0.0095
4	6.7600	0.0063	6.5860	0.0175
5	7.7650	0.0014	7.9100	0.0284
6	8.7380	0.0011	8.8320	0.0018

For the data acquired from HIT, environmental factors and traffic were considered as damaged contributors. With less damage starting from the data collected in January to more damage in the subsequent months, Jan and May were chosen and compared as per Figure 5.4. As a result, the undamaged Fourier spectra for Jan data versus damaged FFT for may data shows that damage is observed in all the six modes, as the amplitude of the damaged (May data) is higher than the amplitude of the undamaged (Jan data). It also shows that frequency is low in the damaged data than the undamaged data as shown in table 4.4 for the first to the fourth mode. This leads to the observation of the time series results as per Figure 5.5.

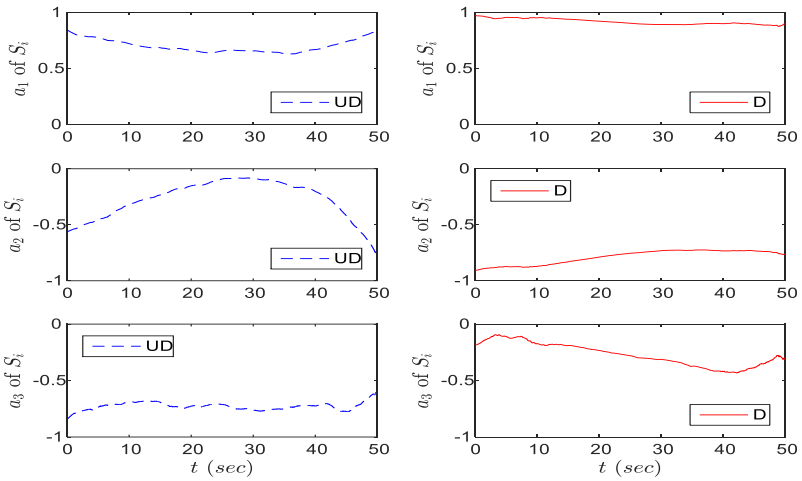

Figure 5.5: Coefficient of a_1, a_2 and a_3 for the UD – Jan vs. D – May data.

For the HIT full-scale study, it is model order 12 which fits, therefore, Figure 5.5 shows the time series of the undamaged (Jan data) and the damaged (May data), adjusted accordingly with the Kalman filter, so as to have the amplitude of the signal with a maximum value of 1, an indication of the correct model being used. The time series shows smooth pattern in the HIT data because unlike model A and model B which were excited by the shaker and damage induced by cutting of the braces, it is the environmental factors which contributed to the bridge damage.

To further observe the performance of the model developed for the HIT data, RMS values for each coefficient under undamaged and damage case is determined so as to measure the energy content in a signal. Therefore, Figure 5.6 is created which shows higher RMS for damaged coefficients 1, 2, 4, 6, 7, 8, 9, 11 and 12.

Since the RMS biggest difference is shown in coefficient a_1 and a_2 in Figure 5.6, they are then plotted for different channels. Thus, Jan, March and May were chosen and compared while plotting coefficient a_1 and a_2 so as to further observe the performance of the model, and that is shown in Figure 5.7 for coefficient a_1 and 5.8 for coefficient a_2 which shows the results with healthy, moderate and significant damage. In both Figures 5.7 and 5.8, comparing January, March and May in each Figure, the month of January that is considered healthy has low RMS in all the channels, but more lower at channel 10 for both Figures. The month of March shows moderate damage but

also very low RMS at channel 10 for both cases. Likewise, the month of May shows significant damage with also very low RMS at channel 10.

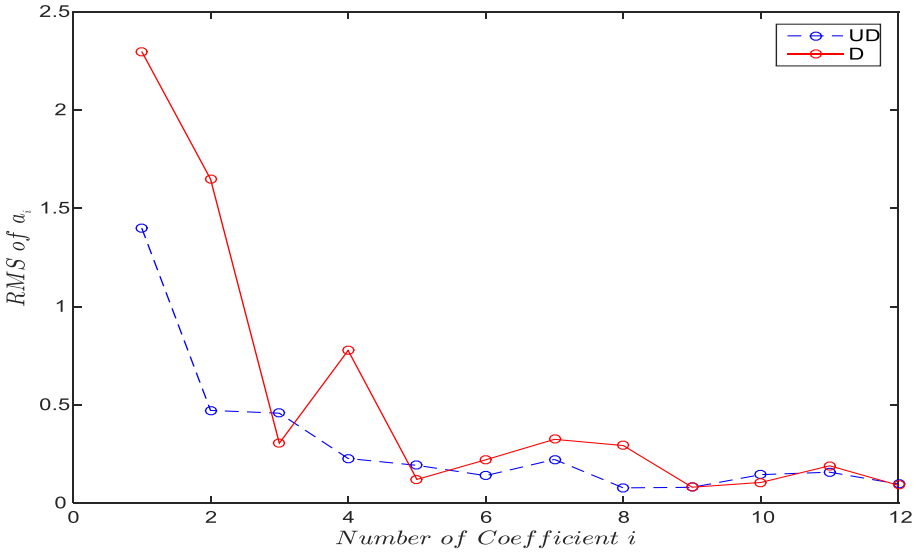

Figure 5.6: RMS Values of TVAR coefficients ai using model order of 12.

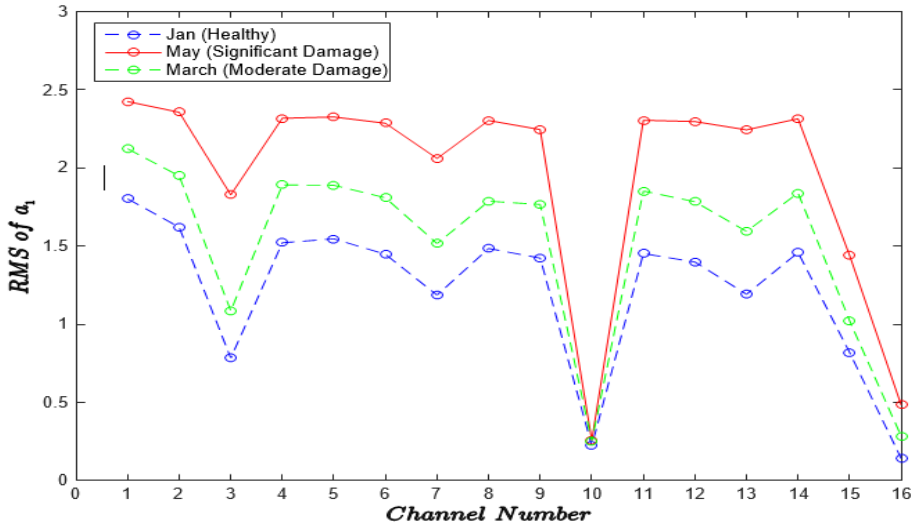

Figure 5.7: RMS values of TVAR coefficients a_1 using model order of 12.

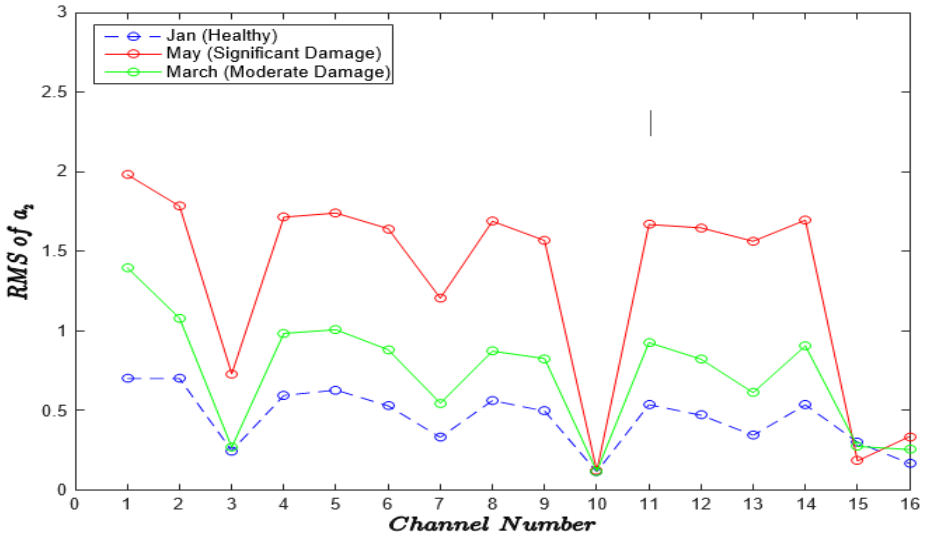

Figure 5.8: RMS values of TVAR coefficients a_2 using model order of 12.

For both Figures 5.7 and 5.8, the main difference is the higher RMS values in all the channels of a_1 than a_2 for the healthy, moderate and significant damage. Since damage is detected in the HIT data, further approach is to determine damage localization whereby a_1 is considered.

5.6. HIT Damage Localization

In addressing the damage localization, RMS percentage difference of May (significant damage) and Jan (healthy) is computed with its results shown in Figure 5.9 which clearly shows that the highest percentage difference is in channel 16, and that should be where the damage is located.

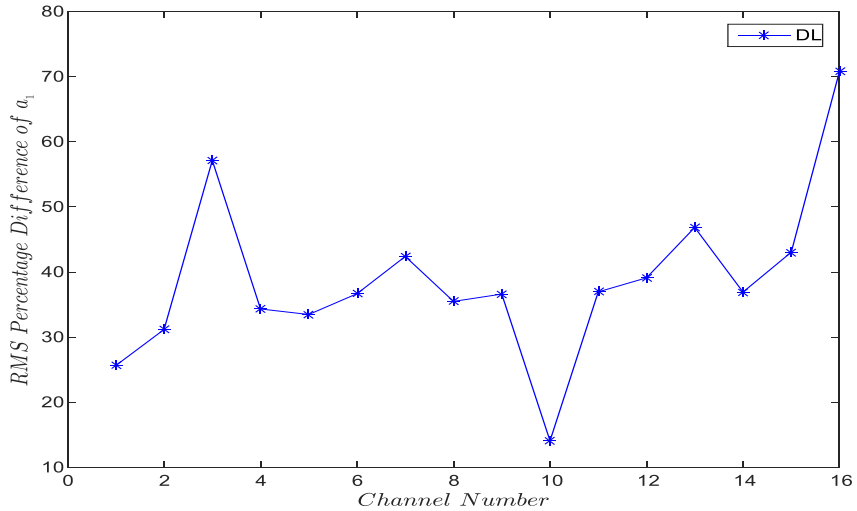

Figure 5.9: RMS percentage difference of TVAR coefficient a_1 for damage localization.

5.7. Conclusion

With the HIT data results, it is fair to say that in overall the model worked as per its intended function in detecting and localizing damage. It seems that for all the cases of coefficients a_1 and a_2 which is considered, it is common for both cases that channel 10 didn't show higher RMS. Further investigation regarding the location of the channel in Figure 5.3 shows that, channel 10 is located right where the bride support is, which should have less vibration. Whereas for the damage localization, it falls right in channel 16 simply because channel 16 is located almost in the middle of the bridge which should exhibit more vibration as there is no support directly underneath the bridge where channel 16 is attached.

6. TECHNIQUE USED FOR COMPARISON

6.1. Stochastic Subspace System Identification

In recent years, system identification of engineering structures such as buildings or bridges has received considerable interest [76]. Through the identification process, the modal characteristics of the observed structures can be determined. System identification methods are well explained by Juang and Ljung in [77, 78]. According to Van Overschee and De Moor [79], among many existing system identification algorithms, N4SID (Numerical Subspace State Space System Identification) identifies the system with an easy parameterization and a fast non-iterative convergence. The N4SID algorithm estimates the structural model in state-space form from which modal properties can be extracted. The algorithm can be applied to systems subjected to known or unknown excitation [80].

6.2. Stochastic Subspace Identification Theory

Mathematically, the system is described in [80] by the following stochastic state-space model:

$$x_{k+1} = Ax_k + Bu_k + w_k \tag{6.1a}$$

$$y_{k+1} = Cx_k + Du_k + v_k \tag{6.1b}$$

where x_k is the state vector, u_k is the vector of input forces, and y_k is the vector of output measurements, and A, B, C, and D are the system matrices of appropriate dimensions to be estimated. w_k and v_k are the process noise and the output measurement noise vectors. Both are assumed to be zero mean, white Gaussian with a covariance matrix as follows:

$$E\left[\begin{pmatrix} w_p \\ v_p \end{pmatrix}\begin{pmatrix} w_q^T & v_q^T \end{pmatrix}\right] = \begin{pmatrix} Q & S \\ S^T & R \end{pmatrix}\delta_{pq} \geq 0, \tag{6.2}$$

where E is the expected value operator. The Kronecker delta δ_{pq} means $\delta_{pq} = 0$ if $p \neq q$, and $\delta_{pq} = 1$ if $p = q$.

The stochastic identification is performed by determining the order n of the system and the system matrices A, C, Q, S, and R. The output measurements are used to construct a block Hankel matrix that can be divided into a past and a future part:

$$Y_{0|2i-1} = \left(\begin{array}{cccc} y_0 & y_1 & \cdots & y_{j-1} \\ y_1 & y_2 & \cdots & y_j \\ \vdots & \vdots & \ddots & \vdots \\ y_{i-1} & y_i & \cdots & y_{i+j-2} \\ \hline y_i & y_{i+1} & \cdots & y_{i+j-1} \\ y_{i+1} & y_{i+2} & \cdots & y_{i+j} \\ \vdots & \vdots & \ddots & \vdots \\ y_{2i-1} & y_{2i} & \cdots & y_{2i+j-2} \end{array}\right) = \left(\frac{Y_{0|i-1}}{Y_{i|2i-1}}\right) = \left(\frac{Y_p}{Y_f}\right) = \frac{past}{future}. \tag{6.3}$$

The subscripts of $Y_{0|2i-1}$ denote the subscript of the first and last element in the first column of the block Hankel matrix. The value of i must be greater than the maximum order of the system that must be identified. For statistical reasons, it is assumed that $j \to \infty$. The Hankel matrix can be divided into 2 parts, Y_p and Y_f, which denote past and future, respectively.

In van Overschee and de Moor [82], P_i is defined as the projection of the row space of the future outputs on the row space of the past outputs as follows:

$$P_i \cong Y_f / Y_p. \tag{6.4}$$

The main stochastic subspace identification theorem states that, the projection P_i is equal to the product of the extended observability matrix Γ_i and the state sequence X_i is represented as,

$$P_i = \Gamma_i X_i = \left(C \quad CA \quad \cdots \quad CA^{i-1}\right)^T \left(x_i \quad x_{i+1} \quad \cdots \quad x_{i+j-1}\right). \tag{6.5}$$

Γ_i and X_i can be extracted using the singular value decomposition (SVD) of the projection P_i as follows:

$$P_i \cong \begin{pmatrix} U_1 & U_2 \end{pmatrix} \begin{pmatrix} S_1 & 0 \\ 0 & 0 \end{pmatrix} \begin{pmatrix} V_1^T \\ V_2^T \end{pmatrix} = U_1 S_1 V_1^T . \tag{6.6}$$

U and V are unitary matrices, and S is a diagonal matrix; U_1, V_1, and S_1 are similar to U, V, and S without their zero singular values. The extended observability matrix Γ_i can be recovered from the SVD of the projection P_i as,

$$\Gamma_i = U_1 S_1^{1/2} . \tag{6.7}$$

The state sequence is the other half of the decomposition.

$$X_i = S_1^{1/2} V_1^T \ . \tag{6.8}$$

The system matrices A and C can be determined in the following system equation:

$$\begin{pmatrix} X_{i+1} \\ Y_{i|i} \end{pmatrix} = \begin{pmatrix} A \\ C \end{pmatrix} (X_i) + \begin{pmatrix} \rho_w \\ \rho_v \end{pmatrix} . \tag{6.9}$$

where $Y_{i|i}$ is a block Hankel matrix with only 1 row of outputs. This set of equations can be easily solved for A and C. Since the Kalman filter residuals ρ_w, ρ_v are uncorrelated with X_i, it is natural to solve the set of equations in a least square approach because the least square residuals are orthogonal and uncorrelated with the regressors X_i.

After identifying the system matrices, the modal analysis is started by performing an eigenvalue decomposition of the system matrix A to obtain the eigen values λ_i and the eigen vectors ψ_i. The modal frequency ω_i and modal damping ξ_i are computed from the following formulas:

$$\lambda_i = -\xi_i \omega_i \pm i \omega_i \sqrt{1-\xi_i^2} = \alpha_i \pm i \beta_i \tag{6.10}$$

$$\text{and } \omega_i = \sqrt{\alpha_i^2 + \beta_i^2}, \quad \xi_i = \frac{\alpha_i}{\sqrt{\alpha_i^2 + \beta_i^2}} . \tag{6.11, 6.12}$$

The mode shape matrix is found from

$$\Phi = C \Psi . \tag{6.13}$$

Finally, in order to assure the quality of the estimated modal vectors, the modal assurance criteria (MAC) are used to measure a consistency between the estimated modal vector and the measured modal vector. The MAC of each mode can be computed from the following equation:

$$MAC_i = \frac{\left(\hat{\psi}_i^T \psi_i\right)^2}{\left(\hat{\psi}_i^T \hat{\psi}_i\right)\left(\psi_i^T \psi_i\right)}. \tag{6.14}$$

where $\hat{\psi}_i$ is the identified modal vector, and ψ_i is the measured modal vector.

The N4SID computations are performed in MATLAB, and the stochastic subspace identification algorithm is implemented using the function N4SID in [83]. It is well known that the accuracy of any system identification technique depends on the level of signal to noise ratio. The modal parameters are identified from structural responses and input forces with the sampling rate.

6.3. Data Analysis

The data used for the N4SID method for comparison is the experimental validation 6-DOF model A, described in section 4.3. The method is used for comparison purposes because it is an important tool that captures the frequency changes. Whereas the TVAR developed captures the changes in the time domain, the N4SID tracks the changes in the frequency domain.

Figure 6.1 shows the acceleration time plot of the raw UD and D data in time domain. The damage acceleration seems dominant because of the excitation of the experimental model through forced vibration using the model shaker and the cutting of the braces. Whereas in Figure 6.2, it shows the data Spectra of the raw UD and D data. The frequencies of the damaged data are more clearly seen than the undamaged data.

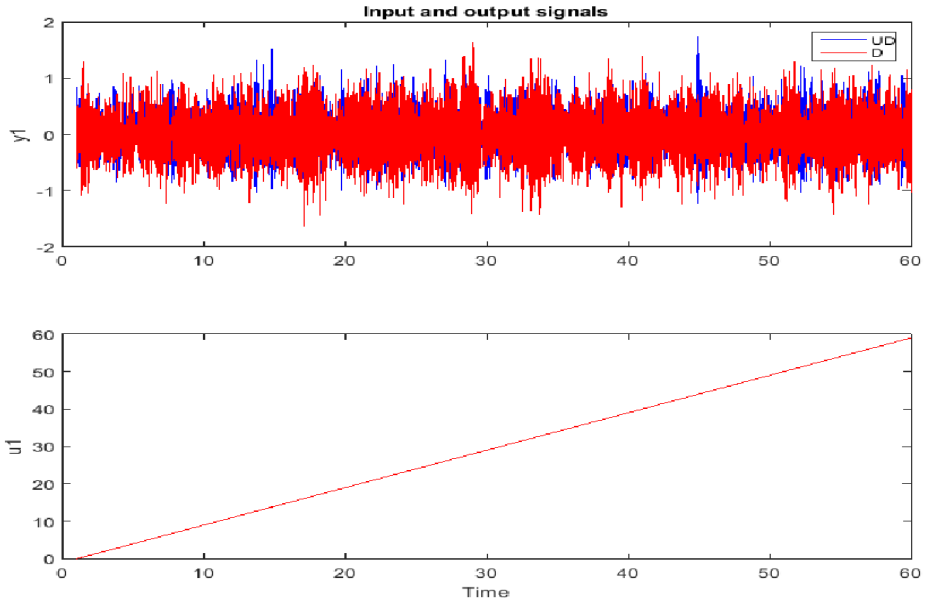

Figure 6.1: Time Plot of the raw UD and D data

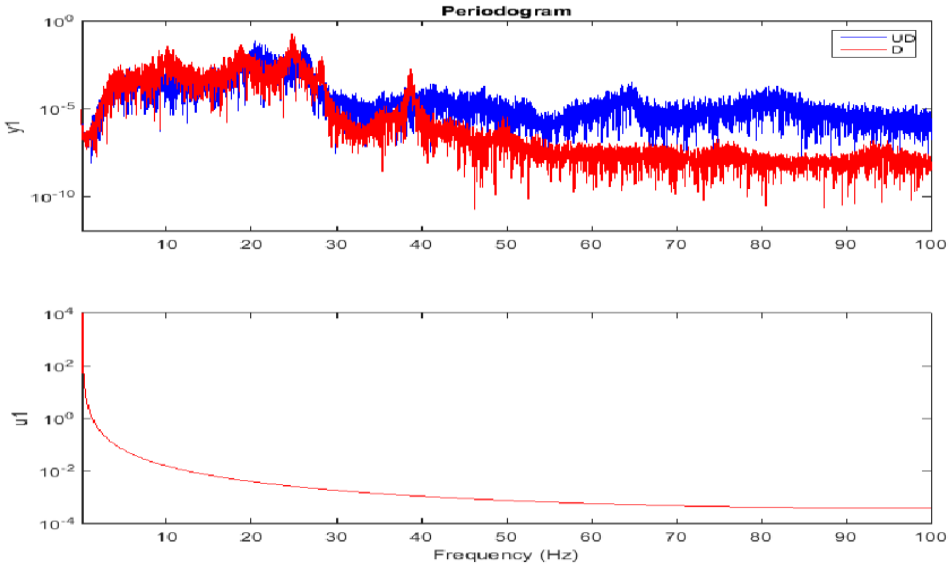

Figure 6.2: Data Spectra of the raw UD and D data

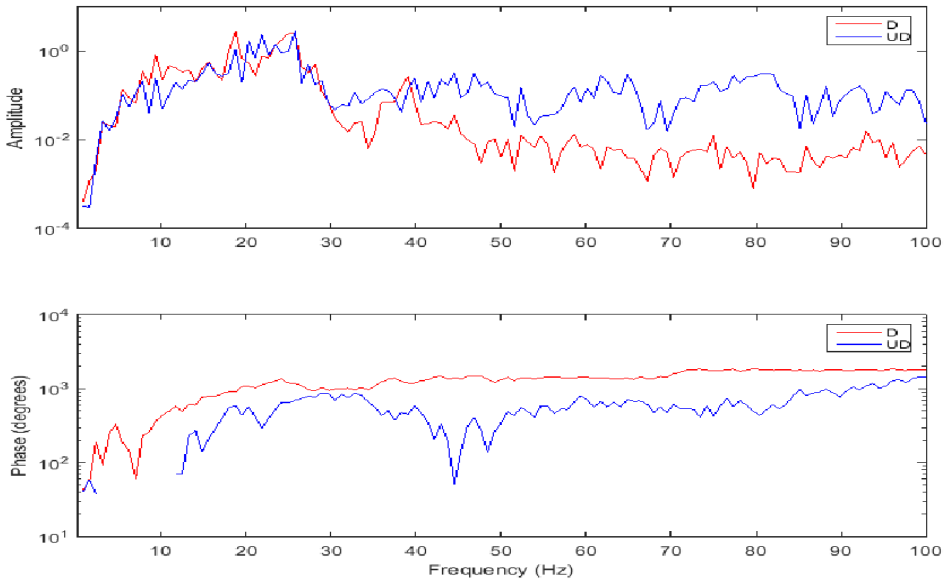

Figure 6.3: Frequency Function of the raw UD and D data

Similarly, Figure 6.3 shows the frequency function of the raw UD and D data. It is clear that after frequency of 48 Hz, there are more visible fluctuations in the D data, similar to what is seen in the application of the TVAR in Figure 4.5.

After preprocessing the data by removing the mean followed by the separation of the data into equal half as model estimation and the model validation, the stochastic subspace method is applied to the data. The reason mean values are subtracted from each signal is to build a linear models that describe the responses for deviations from a physical equilibrium. With steady-state data, it is reasonable to assume that the mean levels of the signals correspond to such equilibrium. Therefore, one can seek models around zero without modeling the absolute equilibrium levels in physical units [84].

According to Peeters and De Roeck [85], an important issue is the determination of the model order. Theoretically, this choice is based on a singular value plot which is one step of the subspace method, but practically, it is more useful to choose the order by considering a

stabilization diagram. The stabilization of the modal parameters can be plotted against the model order. The order where the eigen frequencies, damping ratios and mode shapes remain stable is then selected [85]. Nonetheless, for the model order selection, the model order of 18 that is applied to the main TVAR technique developed is likewise used in the N4SID so as to maintain the model under the same condition for comparison purposes. The application of N4SID with model order 18 resulted into the SSI model response in Figures 6.4 and 6.5.

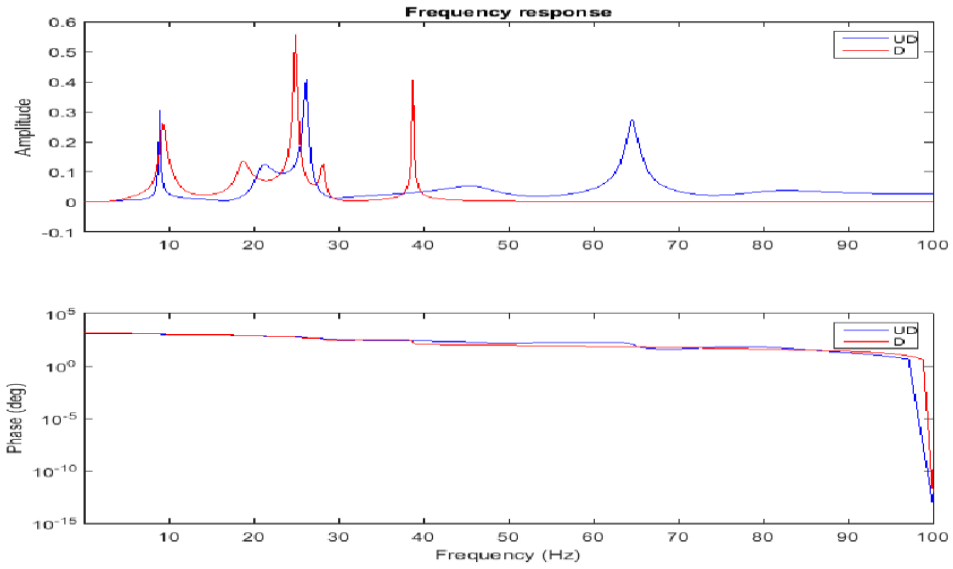

Figure 6.4: N4SID model frequency response for the UD and D data using model order 18

Table 6.1: Frequency response table

	Channel *i*	
Mode	UD ω (Hz)	D ω (Hz)
1	8.911	9.27
2	21.37	18.73
3	26.19	24.90
4	45.14	28.22
5	64.60	38.77
6	82.34	58.19

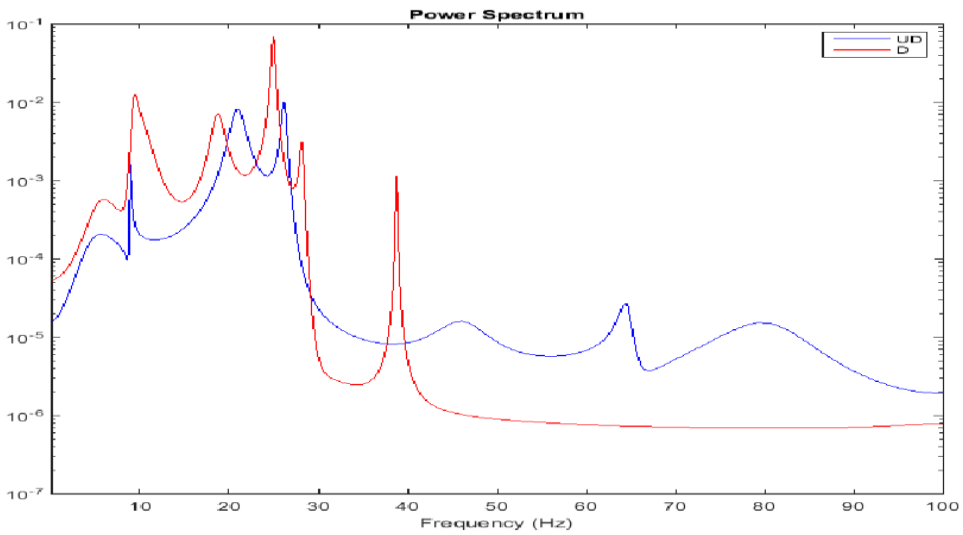

Figure 6.5: N4SID model noise spectrum for the UD and D data using model order 18

Table 6.2: Noise spectrum frequencies

	Channel *i*	
Mode	UD ω (Hz)	D ω (Hz)
1	8.69	5.74
2	20.87	9.42
3	26.25	18.72
4	46.06	24.91
5	64.55	28.18
6	80.51	38.76

Figure 6.4 shows the N4SID model frequency response for the UD and D data, and Figure 6.5 shows N4SID model noise spectrum for the UD and D data. Both N4SID Figures 6.4 and 6.5 shows linear responses and the signal-to-noise ratio is very well represented. In Figure 6.5, the high quality signals with clear peaks in the power spectra are also represented.

On the other hand, the frequency response in Table 6.1 corresponding to Figure 6.4 shows existence of damage in all the frequency modes except for mode 1; whereas in Table 2

corresponding to Figure 6.5, the frequency mode shapes are well represented, as all the six frequency modes for the D is less than the UD modes, a clear indication of damage being represented in the model.

Another useful tool to validate the identified state space model is converting it to theoretical expressions for the output spectra and comparing these spectra with that obtained via FFT on the data [85]. Therefore, in comparing the model frequencies obtained in the SSI and the spectra obtained via FFT on the data in Table 4.1, the frequencies are comparably the same. On the other hand, the SSI technique is able to detect frequencies beyond the natural frequencies obtained using FFT on the data, an indication that it is an important technique that can also be used for damage detection for SHM purposes.

6.4. Conclusions

The effectiveness of the stochastic subspace identification algorithm to estimate modal parameters of the experimental model A is demonstrated. Based on the acceleration responses, the algorithm is capable of identifying natural frequencies and mode shapes of the structure with reasonable accuracy. The algorithm is quite efficient computationally and is therefore implemented using the N4SID function in MATLAB.

7. SUMMARY AND CONCLUSION

In this thesis, a SHM technique is proposed for the purpose of detecting, tracking, and evaluating structural damage and deterioration during in-service condition, as well as extreme events. The study is conducted so as to ardently understand the effective performance of structures, and detect operational anomalies in order to meet the required standards for the SHM. In pursuance of applying the proposed data-driven technique, the data collected on site are essentially paramount. Data inherently used are mainly obtained from experiments, as well as the data acquired from the Harbin Institute of Technology in fulfillment of a full-scale validation. The technique developed is the TVAR model, a method by virtue of its nature is applicable for modeling data whose spectral content varies with time. In a nutshell, TVAR largely consists of a three-step process: state-space modeling of data, employing an adaptive filter framework for dynamic AR model estimation, and using the resulting TVAR model to infer the dynamics of the data. Intrinsically, the AR model is composed of parameters that define the general structure of the model, and the coefficients are realized by fitting the AR model to the data. Therefore, TVAR coefficient time functions need to slowly vary with time so as to have the model achieve the desired spectral representations. Several parametric features including RMS and Kurtosis are used to measure the energy content of a signal, and containing signature of structural damage. Unlike other TVAR-based approaches in the literature, the proposed method is free of any pre-identification step where the vibration data is directly fed into the TVAR modeling. The proposed TVAR technique detects not only the occurrence of structural damage, but also the location of damage. Such damage localization is performed by analyzing relative difference in the energy of the damage and the undamaged coefficients of vibration data. Using both experimental and full-scale studies, it is shown that the proposed TVAR technique can be used effectively to detect and localize damage. For comparison, Stochastic Subspace System Identification (SSI) method is applied to the experimental data. The method is used because it is an important tool that captures the frequency changes, as the SSI

tracks the changes in the frequency domain. Based on the acceleration responses, the algorithm is capable of identifying natural frequencies and mode shapes of the structure with reasonable accuracy. Both techniques can therefore be considered as a useful tool for SHM.

7.1.Future Work

In this thesis, the following are considered as future work:

(1) Write a paper to compare the TVAR technique with the N4SID technique or other techniques on similar structure.

(2) Explore the proposed TVAR technique on pipeline data acquired wirelessly and transmitted remotely to monitor leaks in pipes.

(3) Use the time-series modeling to forecast wind speed for the effective performance of wind turbine and time forecast of solar energy.

(4) Employ the proposed technique on data collected from mechanical equipment such as the gear box and any other oilfield equipment.

REFERENCES

[1] Aktan AE, Brownjohn JMW (2013) Structural identification: opportunities and challenges. ASCE J Struct Eng 139:1639–1647

[2] S. Doebling, C. Farrar, M. Prime and D. Shevitz, Damage identification and health monitoring of structural and mechanical systems from changes in their vibration characteristics: A literature review, Technical Report LA-13070-MS, Los Alamos National Laboratory, Los Alamos, NM, 1996

[3] Y.J. Yan, L. Cheng, Z.Y. Wu and L.H. Yam, Development in vibration-based structural damage detection technique, Mechanical Systems and Signal Processing 19 (2007), 2198–2211

[4] A. Rytter, Vibration based inspection of civil engineering structures, Ph.D. Dissertation, Department of Building Technology and Structural Engineering, Aalborg University, Denmark, 1993

[5] W.J. Staszewski and A.N. Robertson, Time-frequency and time-scale analyses for structural heal monitoring, Philosophical Transction of The Royal Society 365 (2007), 449–477

[6] J.N. Yang, Y. Lei, S. Lin and N. Huang, Hilbert-huang based approach for structural damage detection, Journal of Engineering Mechanics, ASCE 130(1) (2004), 85–95

[7] Khan, M. Advances in Applied Nonlinear Time Series Modeling. PhD thesis, McGill University, 2015. Retrieved from: http://d-nb.info/1073826007/34

[8] Maia, N. and Silva, J. Eds. 1997. Theoretical and experimental modal analysis. Research Studies Press Ltd., Somerset, England

[9] Juang, J.–N., Papa, R.S. 1985. An eigen system realization algorithm for modal parameter identification and model reduction. Journal of Guidance, Control and Dynamics, 8(5): 620-627

[10] James, G.H., Crane, T.G., Lauffer, J.P., and Nord, A.R. 1992. Modal testing using natural excitation. Proceedings of the 10th International Modal Analysis Conference (IMAC), San Diego, USA, pp. 1209-1216

[11] Peeters, B. and De Roeck, G. 2001. Stochastic system identification for operational modal analysis: a review. ASME Journal of Dynamics Systems, Measurement and Control, 123(4): 659-667

[12] K.W. Hipel and A.I. Mcleod, Time Series Modelling of Water Resources and Environmental Systems, Elsevier, Amsterdam, Netherlands, 1994.

[13] A. Sadhu and B. Hazra (2013). "A novel damage detection algorithm using time-series analysis-based blind source separation", *Shock and Vibration*, IOS Press, 20(3): 423-438

[14] Chen, S. R., Cai, C. S. (2007). “Equivalent wheel load approach for slender cable-stayed bridge fatigue assessment under traffic and wind: feasibility study.” Journal of Bridge Engineering, 12(6), 755-764

[15] Li, H. and Ou, J. (2015). "The state of the art in structural health monitoring of cable-stayed bridges." Journal of Civil Structural Health Monitoring, 10.1007/s13349-015-0115-x

[16] Yao R and Pakzad S N 2012 Autoregressive statistical pattern recognition algorithms for damage detection in civil structures Mech. Syst. Signal Process. 31 355–68

[17] Carder, D. S. (1937) “Observed vibrations of bridges”. Bull. Seismol. Soc. Am. 27, 267–303

[18] University of Washington, (1954). “Aerodynamic stability of suspension bridges with special reference to the Tacoma Narrows Bridge.” Bulletin no. 116, University of Washington Engineering Experiment Station, Seattle, Washington

[19] Levy, M., & Salvadori, M. 2002. Why buildings fall down: How structures fail. WW Norton & Company. NY, USA

[20] Public Roads-Winds, Windstorms, and Hurricanes, January/February 2011-FHWA-HRT-11-002. Retrieved from: http://www.fhwa.dot.gov/publications/publicroads/11janfeb/03.cfm

[21] Reza V. F (2013). Structural Health Monitoring and Damage Identification of Bridge Using Triaxial Geophones and Time Series Analysis. Doctoral Dissertation

[22] National Transportation Safety Board (NTSB) (2008). “Collapse of I-35W Highway Bridge, Minneapolis, Minnesota, August 1, 2007.”Accident Report No. NTSB/HAR-08/03

[23] A. S. Usmani, Y. C. Chung, and J. L. Torero. How did the WTC towers collapse: a new theory. Fire Safety Journal, 38(6):501–533, 2003

[24] Doebling, S. W., et al., (1998) "A Review of Damage Identification Methods that Examine Changes in Dynamic Properties,” Shock and Vibration Digest 30 (2), pp. 91-105

[25] Sohn, H. (Hoon), Farrar, C. R. (Charles R.), Hemez, F. M. (François M.), & Czarnecki, J. J. (Jerry J.). (2002). A Review of Structural Health Review of Structural Health Monitoring Literature 1996-2001. United States

[26] Sirca Jr., G.F. and Adeli, H. (2012) System Identification in Structural Engineering. Scientia Iranica, 19, 1355-1364. http://dx.doi.org/10.1016/j.scient.2012.09.002

[27] Boto-Giralda, D., Díaz-Pernas, F.J, González-Ortega, D., Díez-Higuera, J.F., Antón Rodríguez, M. and Martínez-Zarzuela, M. ‘‘Wavelet-based denoising for traffic volume time series forecasting with self-organizing neural networks’’, Computer-Aided Civil and Infrastructure Engineering, 259(7), pp. 530–545 (2010)

[28] Li, H., Huang, Y., Ou, J. and Bao, Y. ‘‘Fractal dimension-based damage detection method for beams with a uniform cross-section’’, Computer-Aided Civil and Infrastructure Engineering, 26(3), pp. 190–206 (2011)

[29] Reuter, U. ‘‘A fuzzy approach for modeling non-stochastic heterogeneous data in engineering based on cluster analysis’’, Integrated Computer-Aided Engineering, 18(3), pp. 281–289 (2011)

[30] Heng, A. S. Y. 2009. Intelligent Prognostics of Machinery Health Utilising Suspended Condition Monitoring Data. Ph.D, Queensland University of Technology

[31] Van Overschee P., De Moor B. 1996. Subspace identification for linear systems: theory, implementation, applications. Kluwer Academic Publishers. Dordrecht, the Netherlands

[32] Alwash, M. Excitation Sources for Structural Health Monitoring of Bridges. PhD Thesis, University of Saskatchewan, 2010

[33] Bendat, J.S. and Piersol, A.G. 1993. Engineering application of correlation and spectral analysis. 2nd Ed. John Wiley and Sons, New York

[34] Farrar, C.R. and James, G.H. 1997. System identification from ambient vibration measurements on a bridge. Journal of Sound and Vibration, 205(1): 1-18

[35] Farrar, C. R., Cornwell, P. J., Doebling, S.W. and Prime, M. B. 2000. Structural health monitoring studies of the Alamosa Canyon and I-40 Bridge. Los Alamos National Laboratory Report LA-13635-MS, New Mexico, U.S.A.

[36] Santamaria, J.C. and Fratta, D. 1998. Introduction to discrete signals and inverse problems in civil engineering. ASCE Press, Virginia, USA

[37] Bao YQ, Li H, Ou JP (2014) Emerging data technology in structural health monitoring: compressive sensing technology. J Civil Struct Health Monit 4(2):77–90

[38] Flamand O, De Oliveira F, Stathopoulos-Vlamis A, Papanikolas P, Panagis A (2014) Using non continuous records from full scale monitoring system for fatigue assessment. In: 7th European workshop on structural health monitoring, Le Cite, Nantes, France, 8–11 July 2014

[39] Ou JP, Li H (2010) Structural health monitoring in mainland China: review and future trends. Struct Health Monit 9:219–231

[40] Transportation Research Board of the National Academies of the USA (2005) Inspection and maintenance of bridge stay cable systems: a synthesis of highway practice, Washington, DC

[41] Li H, Ou JP, Zhou Z (2009) Applications of optical fibre Bragg gratings sensing technology based smart stay cables. Opt Lasers Eng 47:1077–1084

[42] Dascotte E (2011), Vibration monitoring of the Hong Kong Stonecutters Bridge. In: Experimental vibration analysis for civil engineering structures, Varenna, Italy, 3–5 Oct 2011

[43] Zhang R, Duan YF, Wing S, Zhao Y (2014) Smart elasto-magnetoelectric (EME) sensors for stress monitoring of steel cables: design theory and experimental validation. Sensors 14:13644–13660

[44] Zonta D, Esposito P, Pozzi M, Molignoni M, Zandonini R, Wang M, Inaudi D, Posenato D, Glisic B (2012) Monitoring load redistribution in a cable-stayed bridge. In: The 5th European conference on structural control, Genoa, Italy, 18–20 June 2012, Paper No. # 193

[45] Kim CH, Jo BW, Jun JT (2012) Application of laser vibrometer to the measurement and control of cable tensile forces in cablestayed bridges. Int J Distrib Sensor Netw (article ID 810682, 7 pages)

[46] Kurz JH, Laguerre L, Niese F et al (2013) NDT for need based maintenance of bridge cables, ropes and pre-stressed elements. J Civil Struct Health Monit 3:285–295

[47] Qiao GF, Hong Y, Ou JP (2014) Quantitative monitoring of pitting corrosion based on 3-D cellular automata and real-time ENA for RC structures. Measurement 53:270–276

[48] Zhao XF, Cui YJ, Wei HM, Kong XL, Zhang PL, Sun CS (2013) Research on corrosion detection for steel reinforced concrete structures using fiber optical white light interferometer sensing technique. Smart Mater Struct 22(6):512–519

[49] Li H, Ou JP (2005) Design approach of health monitoring system for cable-stayed bridges. I: Proceedings of the 2nd international conference of structural health monitoring for intelligent infrastructure, Shenzhen, China, 13–16 Nov 2005

[50] Anderegg P, Bronnimann R, Meier U (2014) Reliability of longterm monitoring data. J Civil Struct Health Monit 4:69–75

[51] Dincer S, Aydın E, Gencer H. A Real-Time Instrumentation Approach for Structural Health Monitoring of Bridges. Proceedings of the Istanbul Bridge Conference, 201

[52] Subba Rao, T. (1970). The fitting of non-stationary time-series models with time dependent parameters. Journal of the Royal Statistical Society, Series B (Methodological), 32(2), 312-322

[53] Chen, L. Vector Time-Varying Autoregressive (TVAR) Models and their Application to Downburst Wind Speeds. PhD thesis, Texas Tech University, 2005

[54] Musafere F, Sadhu A and Liu K 2015 Towards damage detection using blind source separation integrated with time-varying auto-regressive modeling Smart Mater. Struct. 25 015013

[55] Dahlhaus, R. and Sahm M. (2000). Likelihood methods for nonstationary time series and random fields. Resenhas Journal, 4, 457-477

[56] Kitagawa, G., and Gersch, W. (1985). A smoothness priors time-varying AR coefficient modeling of nonstationary covariance time series. IEEE Transactions on Automatic Control, AC-30(1), 48-56

[57] Akaike, H. (1969). Fitting autoregressive models for prediction. Annals of the Institute of statistical Mathematics. 21, 243–247

[58] M. Niedwiecki, Identification of Time-varying Processes, John Wiley & Sons, Chichester, England, 2000

[59] Akaike, H. (1970). Statistical predictor identification. Ann. Inst. Statist. Math. 22, 203- 217.

[60] Akaike, H. (1974). A new look at the statistical model identification. IEEE Trans. Automat. Control, AC-19, 716-722

[61] Schwarz, G. (1978). Estimating the dimension of a model. Ann Stat, 6, 461-464

[62] Percival DB, Walden AT. Spectral analysis for physical applications: multitaper and conventional univariate techniques. Cambridge University Press; Cambridge; New York, NY, USA: 1993

[63] Arnold M, Miltner WHR, Witte H, Bauer R, Braun C. Adaptive AR modeling of nonstationary time series by means of Kalman filtering. IEEE Trans. Biomed. Eng. 1998; 45:553–62. [PubMed]

[64] David P. Nguyen, Matthew A. Wilson, Emery N. Brown, Riccardo Barbieri
J Neurosci Methods. Author manuscript; available in PMC 2010 Nov 15. Retrieved from: http://www.ncbi.nlm.nih.gov/pmc/articles/PMC2767386/

[65] Nguyen D 2009 Measuring instantaneous frequency of local field potential oscillations using the Kalman smooth *J. Neurosci. Method* 187 365–7

[66] Box GEP, Jenkins GM, Reinsel GC. Time series analysis: forecasting and control. 4th ed. John Wiley; Hoboken, N.J.: 2008

[67] Oppenheim AV, Schafer RW, Buck JR. Discrete-time signal processing. 2nd ed. Prentice Hall; Upper Saddle River, N.J.: 1999

[68] Feng L, Yi X, Zhu D, Xie X and Wang Y 2015 Damage detection of metro tunnel structure through transmissibility function and cross correlation analysis using local excitation and measurement *Mech. Syst. Signal Process.* 60–1 59–74

[69] Garcia D and Trendafilova I 2014 A multivariate data analysis approach towards vibration analysis and vibration-based damage assessment: application for delamination detection in a composite beam*J. Sound Vib.* 333 7036–50

[70] Mosavi A., Dickey D., Seracino R.,Rizkalla S. (2011). "Identifying damage locations under ambient vibrations utilizing vector autoregressive models and Mahalanobis distances", Mechanical Systems and Signal Processing, Vol. 26, No. 0, pp. 254–267

[71] RAO S.S.*, Mechanical Vibrations*, Prentice Hall PTR, NJ, 2011

[72] Zhou., W. (2008). *SHM Benchmark Problem*. Center of Structural Monitoring and Control of the Harbin Institute of Technology. Accessed from: http://smc.hit.edu.cn/

[73] Li S, Li H, Liu Y, Lan C, Zhou W, Ou J. SMC structural health monitoring benchmark problem using monitored data from an actual cable-stayed bridges. *Structural Control and Health Monitoring* 2013. DOI:10.1002/stc.1559

[74] He, L., Lian, J., Ma, B., and Wang, H. (2014), "Optimal multiaxial sensor placement for modal identification of large structures," Struct. Control. Hlth., 21(1), 61-79

[75] Li H, Zhou WS, Ou JP, et al. A study on system integration technique of intelligent monitoring systems for soundness of long span bridges. China Civil Engineering Journal 2006; 39(2):46–52

[76] Cunha, A., Caetano, E., Magalhaes, F., and Moutinho, C. (2006). From input output to output-only modal identification of civil engineering structures. Structural Assessment Monitoring and Control [SAMCO] Final Report 2006. F11 Selected Papers. Available from: www.samco.org. Accessed date: May 6, 2008.

[77] Juang J.N. (1994). Applied System Identification. 1st ed. Prentice-Hall, Englewood Cliffs, NJ, USA, 352p.

[78] Ljung, L. (1999). System Identification: Theory for the User. 2nd ed. Prentice-Hall, Englewood Cliffs, NJ, USA, 248p.

[79] Van Overschee, P. and De Moor, B. (1994). N4SID: Subspace algorithms for the identification of combined deterministic-stochastic systems. Automatica, 30(1):75-93.

[80] Jiravacharadet, M. (2008). Stochastic Subspace System Identification of a Multi story Building. Suranaree J. Sci. Technol. Vol. 15 No. 4; October - December 2008

[81] Brincker, R. and Andersen, P. 2006. Understanding Stochastic Subspace Identification. Proceeding of the 24th IMAC.

[82] Van Overschee, P. and De Moor, B. (1996). Subspace Identification for Linear Systems: Theory, Implementation, Applications. 1st ed. Kluwer Academic Publishers, Boston, Mass., USA, 254p.

[83] Ljung, L. (2002). System Identification Toolbox: User's Guide. 1st ed. Mathwork Inc., Natick, MA, USA, 384p.

[84] MathWorks. (2017). Identify Linear Models Using System Identification App. Retrieved from: https://www.mathworks.com/help/ident/gs/identify-linear-models-using-the-gui.html

[85] B. Peeters, G. De Roeck, “Stochastic subspace system identification of a steel transmitter mast”, In Proceedings of IMAC 16, the International Modal Analysis Conference, pp. 130-136, Santa Barbara, USA, February 1998.